

NPS ARCHIVE
1958.06
GLOWICKI, W.

PHOTOELASTIC INVESTIGATION OF
SHEAR STRESSES IN COFFERDAMS

WALTER F. GLOWICKI

DUDLEY KNOX LIBRARY
NAVAL POSTGRADUATE SCHOOL
MONTEREY CA 93943-5101



PHOTOELASTIC INVESTIGATION OF SHEAR STRESSES IN COFFERDAMS

by

CAPTAIN WALTER F. GLOWICKI

UNITED STATES MARINE CORPS

A Thesis Submitted to the Faculty
of the Department of Civil Engineering
in Partial Fulfillment of the
Requirements for the Degree of
MASTER OF CIVIL ENGINEERING

NPS ARCHIVE

1958.06

GLOWITZKE, W.

TABLE OF CONTENTS

	LIST OF TABLES	Page v
	LIST OF FIGURES	vi
	FORWARD	viii
	ABSTRACT	x
I.	INTRODUCTION	1
	A. Historical Review	1
	B. Statement of Problem	4
II.	THEORY	5
	A. Concepts by Terzaghi	5
	B. Concepts by Cummings	10
	C. Concepts by Verdeyen	16
	D. Concepts by Packshaw	22
	E. Photoelasticity	25
III.	APPARATUS	28
	A. Polariscopes	28
	B. Load Application Device	28
	C. Models	30
	D. Photographic Equipment	33
	E. Materials	33
IV.	METHOD OF PROCEDURE	34
	A. Preliminary Phase	34
	B. Final Phase	37
	C. Developing Procedure	40
	D. Printing Procedure	40
V.	RESULTS AND DISCUSSION	41

VI.	CONCLUSIONS	72
VII.	RECOMMENDATIONS	74
VIII.	LITERATURE CITED	75
IX.	APPENDIX	78

LIST OF TABLES

	Page
Table 1 Raw Data - Test 1	78
Table 2 Raw Data - Test 2	80
Table 3 Raw Data - Test 3	81
Table 4 Raw Data - Test 4	83
Table 5 Raw Data - Test 5	85

LIST OF FIGURES

	Page
Figure I Deflection of Cellular Cofferdams	7
Figure II Cellular Cofferdam on Rock	8
Figure III Pressure Diagram	8
Figure IV Cellular Cofferdam on Rock	11
Figure V Tilting Failure of a Cellular Cofferdam	11
Figure VI Dimensions and Lines of Action of Forces Used in the Derivations	12
Figure VII Pressure Diagram	15
Figure VIII Cellular Cofferdam on Rock	17
Figure IX Pressure Distribution	17
Figure X Cellular Cofferdam on Rock (Flexible Walls) ...	19
Figure XI Pressure Distribution	19
Figure XII Rupture Plane for Pressure and Resistance	23
Figure XIII Pressure and Resistance Diagrams	23
Figure XIV Plane Polariscope	27
Figure XV Circular Polariscope	27
Figure XVI Elements of the Polariscope	29
Figure XVII Loading Device	31
Figure XVIII Cofferdam Models	32
Figure XIX Full View of Experimental Setup	38
Figure XX Photographic Results - Test 1	42
Figure XXI Load and Yield Curve - Test 1	46
Figure XXII Photographic Results - Test 2	49
Figure XXIII Load and Yield Curve - Test 2	53

Figure XXIV	Photographic Results - Test 3	55
Figure XXV	Load and Yield Curve - Test 3	58
Figure XXVI	Photographic Results - Test 4	61
Figure XXVII	Load and Yield Curve - Test 4	65
Figure XXVIII	Photographic Results - Test 5	67
Figure XXIX	Load and Yield Curve - Test 5	71
Figure XXX	Calibration Curve	87

FOREWARD

The incentive for undertaking this investigation was given during a discussion with Associate Professor S. V. Best of the Department of Soil Mechanics.

Further impetus was presented during the Graduate Foundation Course conducted by Assistant Professor R. L. Shiffman. During the course of instruction it was revealed that additional information is needed in order to fully understand the nature of shear stresses within the fill material of cellular cofferdams.

The writer desires to express his sincere appreciation to Professor S. V. Best for providing guidance, stimulating interest for further exploration and encouragement when needed.

Gratitude is also expressed to Assistant Professor E. A. Fox, of the Department of Mechanics, for his assistance on matters pertaining to photoelasticity and photoelastic material.

The author is deeply indebted to Assistant Professor L. W. Thrasher, of the Department of Engineering Drawing for his thorough indoctrination on the technique of developing and printing of photographic films.

Appreciation is also expressed to Professor G. R. Shaw of the Department of Civil Engineering, for the use of the dark room and photographic equipment.

The complete cooperation of the Department of Mechanics, particularly Assistant Professor C. S. Barton for the use of the polariscope is deeply appreciated.

Appreciation is also expressed to Assistant Professor R. L. Shiffman for his recommendations in connection with the preparation of the manuscript and for the use of his Graflex camera.

The author is deeply indebted to his wife for her patience, encouragement and suggestive criticism in the preparation of the manuscript.

ABSTRACT

The distribution of shear stresses within the granular fill material of a cofferdam is qualitatively investigated by utilizing the science of photoelasticity and assumed ideal conditions.

A brief history of the study of internal shear considerations is presented accompanied by a condensed history of achievements made by the application of photoelasticity to the study of soils in general.

Three theoretical concepts related to the distribution of internal stresses within cellular cofferdams together with a concept pertaining to a double wall cofferdam are summarized. In addition there is included a brief explanation of the theory of photoelasticity and the essential elements of a polariscope.

The original apparatus developed, and subsequent modifications are discussed in detail.

Preliminary testing procedures and difficulties encountered are described in detail. The final testing procedure adopted is summarized.

Results, for the five tests, are presented in the form of a series of photographs and curves. Tests were performed with the fill material being placed in a dense and loose state respectively.

The test results are evaluated and appropriate general conclusions are listed.

Methods of minimizing or eliminating experimental difficulties are presented in the recommendations.

PART I

INTRODUCTION

A. HISTORICAL REVIEW

Since the beginning of time man has been trying to hold back the waters. Through the ages various methods and materials have been utilized for this purpose. At the present time one of the structures utilized for this purpose is the cellular cofferdam.

A cofferdam is a temporary structure built for the purpose of excluding earth and water from an excavation in order that work may be done in relatively dry conditions.

A cellular cofferdam consists of interconnected cells made up of interlocking steel sheet piling which are subsequently filled with granular soil. Since they are used where the area to be excavated is of considerable extent, the cells are designed as selfstable units.

The first cellular cofferdam was built at Block Rock Harbor, New York, at the turn of the century (19).

In 1910, cellular construction was utilized in the salvaging operations of the battleship Maine in Cuba. Since that time cellular cofferdams have become increasingly common because they provide satisfactory service and are economical where large lateral pressures are encountered. Through the years, experience and investigation have continually presented the designer more vivid conceptions of the factors which determine the stability of these necessary structures.

The granular fill placed within a cellular cofferdam not only provides stability but is also one of the means of failure of a cofferdam - that is - by shear deformations created by inward tilting.

Internal shear consideration was initially considered by the T. V. A. Engineers in the early 30's (19).

Subsequently an attempt was made by Pennoyer (13) in 1934 to explain mathematically occasional leaning or distortion of the cells because of evident lack of internal shear resistance of the soil in the cells.

In 1945, a valuable and significant contribution was presented by Karl Terzaghi (19). It contained an extensive discussion and methods of analysis on the rational design procedure and behavior exhibited by cellular cofferdam construction.

A method of analysis to determine the distribution of pressure within cellular construction was presented by Professor J. Verdeyen in 1948 (21).

Recently, a paper published by E. H. Cumming (4) presents a new concept as to the mode of failure of cofferdams as a result of insufficient internal shear resistance.

Photoelasticity was first introduced to the engineering world at the turn of the century by Professors E. G. Coker and L. N. G. Filon of the University of London (10). However, it was not until the early 1930's that photoelasticity was applied to the study of soils.

Photoelastic patterns of stress distributions under footings were described in a bulletin published by Professor W. S. Housel in 1929 (9).

Four years later an investigation was conducted by a committee of the American Society of Civil Engineers, to visualize the stresses acting in a foundation and its supporting ground. The "bulb of pressure" in the supporting ground was visualized by using a polariscope and bakelite model (15).

In 1935, a photoelastic investigation was conducted which presented the points of high stresses and general behavior of shrinkage stresses in masonry dams by utilizing a bakelite model (17). Also in 1935 an extensive mathematical solution, in connection with problems in plane stress and plane strain, was applied to the photoelastic analysis of dams by John H. Brahtz (2).

In 1940 Messers. Farquharson and Hennes conducted experiments in order to provide engineers with a record of experimental difficulties encountered and procedures evolved to overcome the difficulties in utilizing gelatin models for photoelastic analysis of stress distribution in earth masses (9).

The distribution of stresses and their relative order of magnitude in soil slopes was the primary objective of an investigation conducted by EK-KHOO-TAN in 1948 (18).

The most recent use of photoelastic methods in the analysis of soils was presented by Dantu (6). This investigation was aimed at understanding the manner of stress transmission and the geometrical and statistical structure of non-cohesive masses.

B. STATEMENT OF PROBLEM

Previous discussions reveal that, at the present time, there are several concepts which vary in detail as to the manner in which stresses are transmitted in a cofferdam subject to tilting.

It is readily realized that the exact analysis of the behavior of the fill material within a cofferdam is highly indeterminate, if not impossible. However, by assuming an idealized condition it becomes possible to demonstrate the distribution of stresses with some assurance.

Recent contributions in the understanding of the complex behavior of soils, have resulted from a concentrated effort of utilizing all available knowledge regarding fundamental phenomenon in the solution of any soil problem.

One of the useful tools presently available for the determination of stress concentration in statically indeterminate structures is the science of photoelasticity.

In view of the above, and the fact that no previous work of this nature has been called to the attention of the author an attempt is hereby made to initiate and develop a simple technique and procedure to investigate shear stresses in cofferdams and to visualize the distribution of stresses in a cofferdam in order to provide some additional information on such a highly complex and indeterminate problem.

PART II

THEORY

Previous considerations indicate that the exact calculations of cofferdams is difficult and complex. As a result, numerous theories dating back to 1931 have been published.

Generally the analysis for the stability of a cofferdam includes considerations relative to (1) general stability, (2) resistance provided at the joints and (3) the state of equilibrium of the fill material and drainage.

Since this thesis is primarily concerned with the internal stability of the fill material, the author has summarized the internal stability considerations as presented by Messers. Karl Terzaghi (19), E. M. Cummings (4), Jacques Verdeyen (21), and Packshaw (19).

For detailed considerations and discussions the reader is referred to the respective references.

A. CONCEPTS BY TERZAGHI

In 1945, Karl Terzaghi emphasized the fact that one of the ways in which a cofferdam may fail is by the shear deformation created by inward tilt. Field experience indicated that the horizontal deflection of the crest can be slightly larger than ten percent of the height of the structure without causing structural injury to the cofferdam.

According to Terzaghi the horizontal deflection depends on the elastic properties of the fill in the cofferdam, and that the

relation between the unbalanced horizontal pressure and the corresponding deflection is similar to the relation between stress and strains in soil in general. The strains in a soil increase approximately with the square of the stress whereas the deflection of the crest increases roughly with the square of the unbalanced horizontal pressure. As shown in Figure I, both the strains in the soil and deflection of the crest increase at a slowly decreasing rate under constant stress or pressure conditions. This was demonstrated by I. A. Rimstad (18).

The analysis is based on the assumptions that the distribution of pressure at the base of a cellular cofferdam resting on rock, as shown in Figure II is such as shown by the line xy in Figure III, and the shear stresses acting at the contact surface, between the fill and sheet piles prior to the application of the overturning moment M , are disregarded.

The shaded area in Figure III indicate the stresses on the base due to the overturning moment M . If the area of each shaded triangle is represented by Q we can write the expression

$$M = \frac{2}{3} b Q \quad \text{or} \quad Q = \frac{3}{2} \frac{M}{b} \quad (1)$$

where in the external applied moment is resisted by the internal couple with force Q and a lever arm of $\frac{2b}{3}$

Static equilibrium requires that the total shear force on the neutral plane GK per unit length of the cofferdam must be equal to Q . The shearing resistance S per unit length of the dam on this plane must be equal to the product of the earth pressure

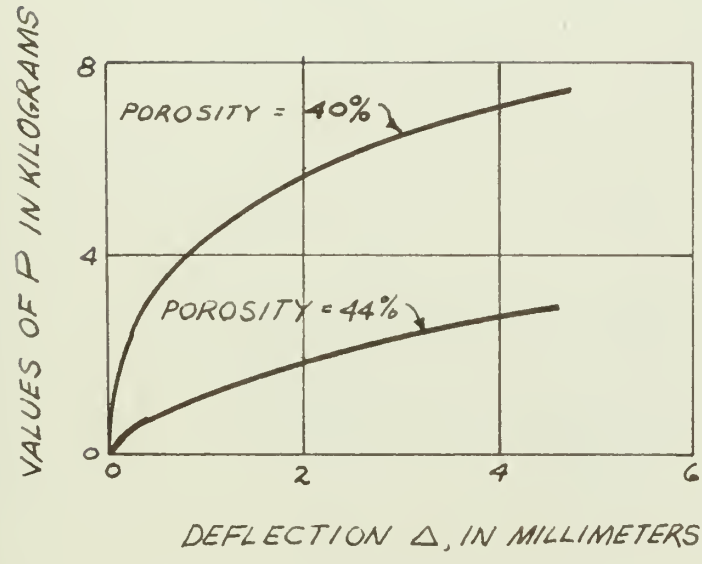
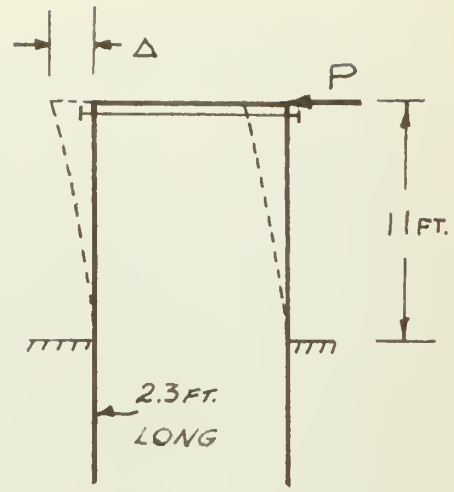


FIGURE I DEFLECTION OF CELLULAR COFFERDAMS

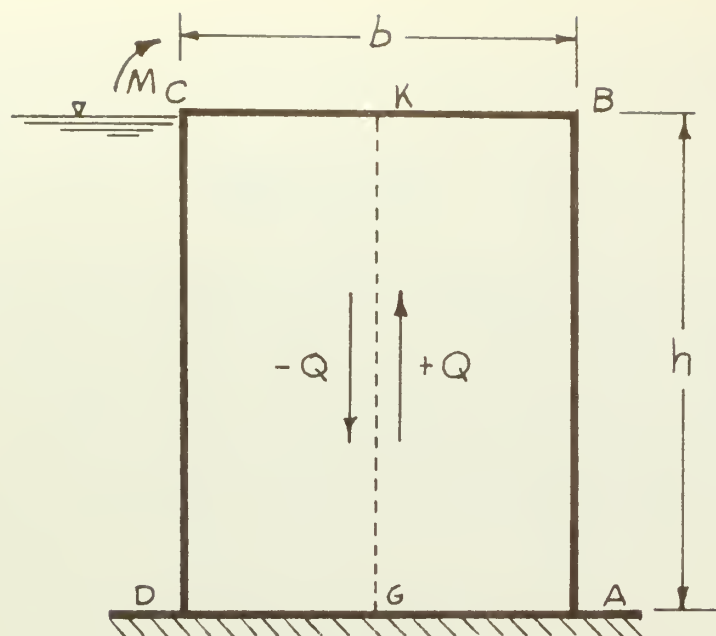


FIGURE II CELLULAR COFFERDAM
ON ROCK

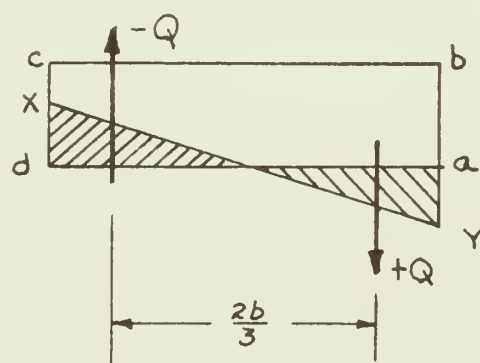


FIGURE III PRESSURE DIAGRAM

p and the coefficient of internal friction of the soil. The earth pressure per unit of area of vertical section at depth z is expressed by

$$p = w z C \quad (2)$$

where w is the unit weight of the soil and C is an empirical constant commonly referred to as the coefficient of earth pressure. Since the pressure distribution is assumed to be hydrostatic, the total earth pressure P on plane GK per unit length of the dam is represented by

$$P = \frac{1}{2} w C h^2 \quad (3)$$

where h is the height of the cofferdam. Therefore the shearing resistance S is expressed by

$$S = P \tan \phi = \frac{1}{2} w C h^2 \tan \phi \quad (4)$$

This shearing resistance is augmented by the friction in the interlocks because no failure by shear along GK , can occur without simultaneous slippage of the interlocks in the plane.

Terzaghi concluded that the shear resistance through the fill in a cellular cofferdam and lock friction at best can only be estimated because of the complex nature of the factors involved.

B. CONCEPTS BY E. M. CUMMINGS

The following discussion is based on the assumptions that the stability of a cellular cofferdam against failure by tilting depends largely upon the horizontal shear resistance of the fill material and that the moment of resistance against tilting remains constant for external loads which may be represented by a triangular pressure diagram.

Figure IV presents a sand filled cellular cofferdam resting on a horizontal rock base, which has tilted due to lateral pressure as indicated by dotted lines. Line AE represents a plane at the angle of internal friction ϕ . The shear resistance on plane AE is equal to the tendency of the fill above to slide on AE. As the cofferdam tilts point E moves to E', and the new plane A'E makes an angle ϕ' with the base. Since $\phi' > \phi$ the fill above A'E slides down a steeper slope. The fill below AE is transformed into a passive state by the lateral thrust and the fill above AE acts as a surcharge.

Figure V represents the tilting failure of a cellular cofferdam by sliding on planes parallel to the rock base.

The dimensions and lines of action of forces acting are shown in Figure VI (a). Since the fill above AE slides when the cofferdam tilts no internal lateral resistance is accumulated between the top of the cofferdam at C and point E. The sheet piles, stiffened by the fill above E merely transmit forces which are applied above point E to the completely confined material within the prism AED.

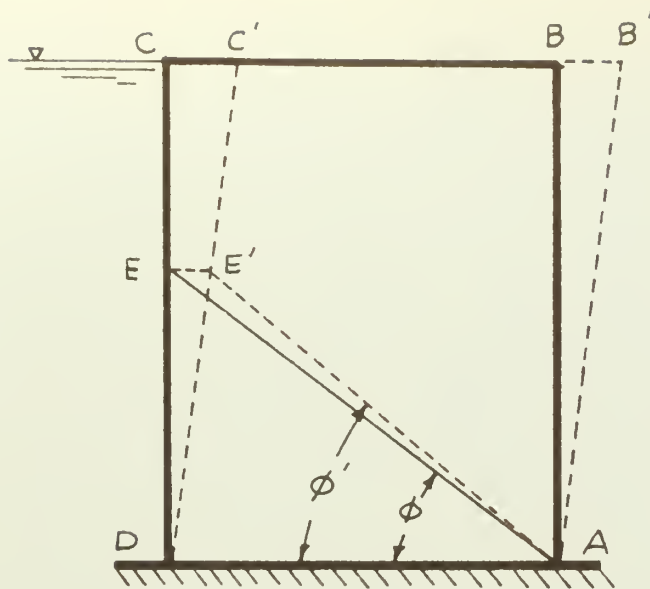


FIGURE IV

CELLULAR COFFERDAM
ON ROCK

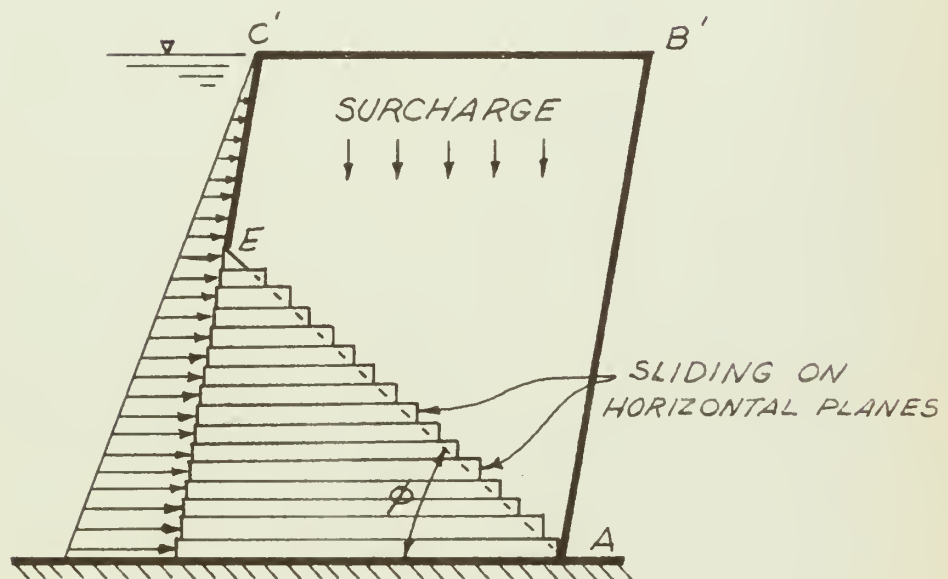
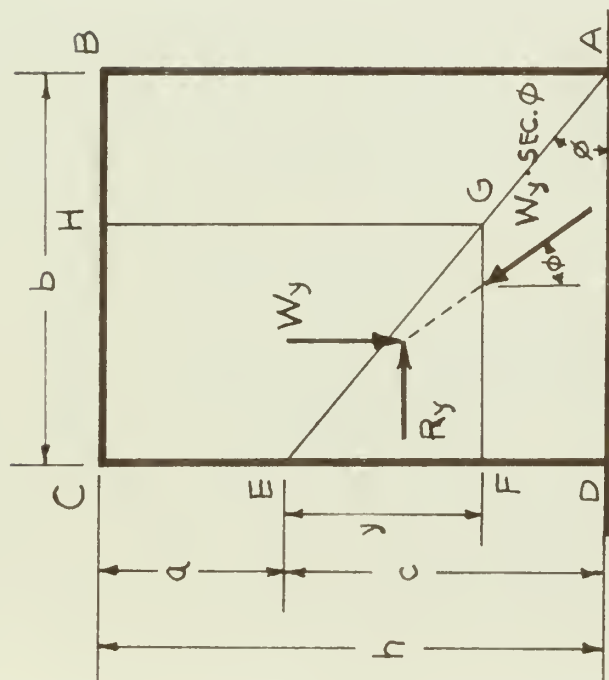
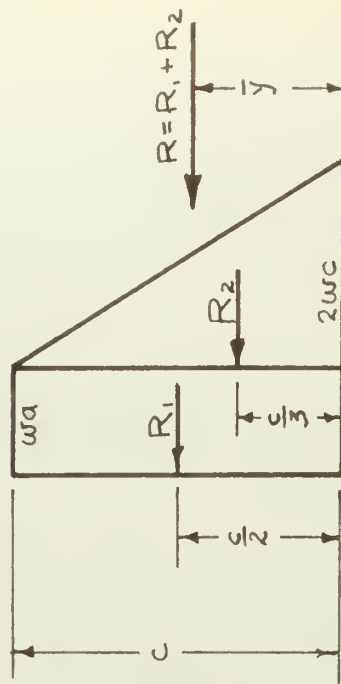


FIGURE V

TILTING FAILURE OF A
CELLULAR COFFERDAM



(a)



(b)

FIGURE VI DIMENSIONS AND LINES OF ACTION OF FORCES USED IN THE DERIVATIONS

In developing the ultimate lateral shear resistance at any depth y below E , force R_y is equivalent to the resistance to sliding of prism $CFGH$ on plane FG , which in turn is equal to the product of the weight W_y of the prism and the tangent of the angle of internal friction ϕ .

$$\text{Thus} \quad R_y = W_y \tan \phi \quad (5)$$

and $W_y = w(a + y)y \cot \phi$, where w is the unit weight of the fill material, therefore

$$R_y = w(ay + y^2) \quad (6)$$

The force R which develops the ultimate lateral shear resistance of the entire cell is obtained by substituting $y = c$.

$$\text{Therefore} \quad R = w(ac + c^2) \quad (7)$$

$$\text{where} \quad c = b \tan \phi \text{ and } a = h - c$$

The equation is represented graphically in Figure VI (b).

The area of this diagram is equal to R . Summation of moments about the base of the cofferdam shows that the moment of resistance M_s is expressed by

$$M_s = R_1 \frac{c}{2} + R_2 \frac{c}{3} \quad (8)$$

$$\text{or} \quad M_s = wac \left(\frac{c}{2} \right) + wc^2 \left(\frac{c}{3} \right) \quad (9)$$

$$\text{where} \quad M_s = w \left(\frac{ac^2}{2} + \frac{c^3}{3} \right) \quad (10)$$

Since the lateral force R , which develops the maximum lateral resistance, is equal to the weight of the fill within the cell times the tangent of the angle of internal friction we can write

$$R = wbh \tan \phi \quad (11)$$

The height \bar{y} of the resultant R above the base may be

found as follows

$$\bar{y} = \frac{M_s}{R} = \frac{M_s}{wbh \tan \phi} \quad (12)$$

The internal and external pressure distributions assumed are shown in Figure VII.

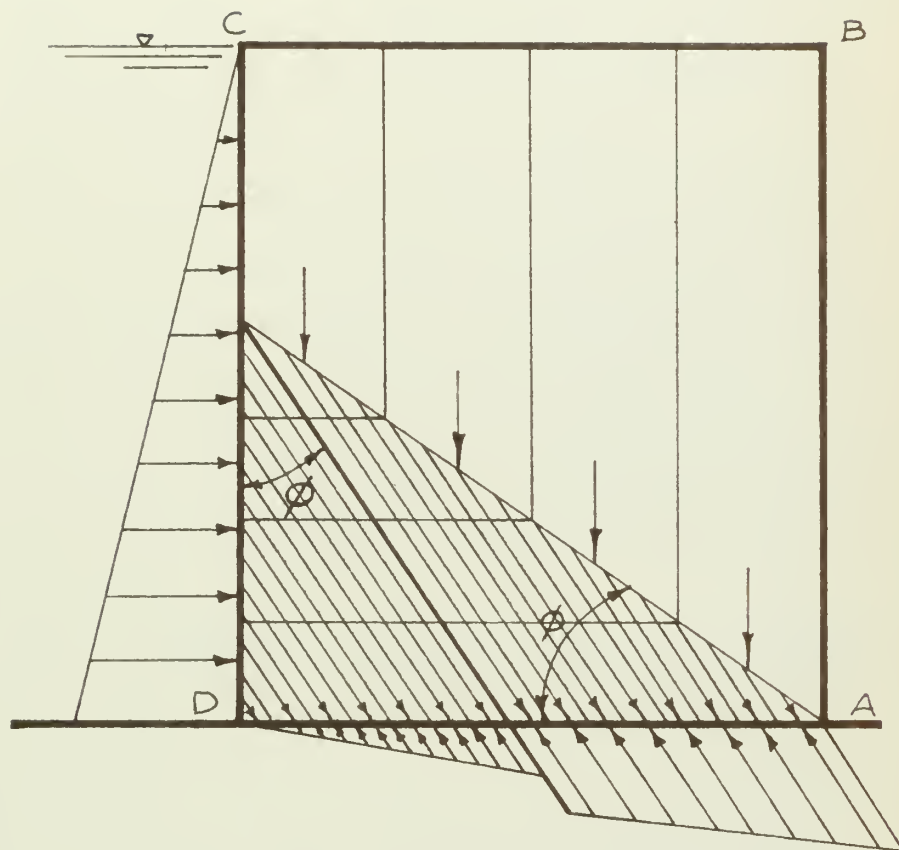


FIGURE VII PRESSURE DIAGRAM

C. CONCEPTS BY JACQUES VERDEYEN

A discussion as presented by Verdeyen in reference (21) is based on the following assumptions:

1. The walls are inflexible.
2. The thrusts and counter thrusts of earth occur in a manner similar to the Coulomb Theory.
3. Movements of the walls are similar to rotations around their base.
4. The slip plane is the same as that which is produced in soil of indefinite length only retained by a wall.

A cellular cofferdam subject to a lateral thrust W tilts in a manner shown in Figure VIII and assumes the shape $AB'C'D$. Equilibrium must be established between the resultant P , which is the weight of prism ABE , the pressure Ea on wall AE and force Q acting on slip plane AE .

The external thrust W is counterbalanced by the resultant of the passive pressures which may develop along CD and which arise from prism $AECD$.

The distribution of active pressure on wall AB is shown in Figure IX (b). Possible distribution of passive earth pressure on wall CD is shown in Figure IX a(2). The external pressure diagram on wall CD is represented by triangle CDD' in Figure IX a.

According to Verdeyen these pressure distributions are not applicable to cellular structures because the walls which form them have slight stiffness and in addition the sheet piles become

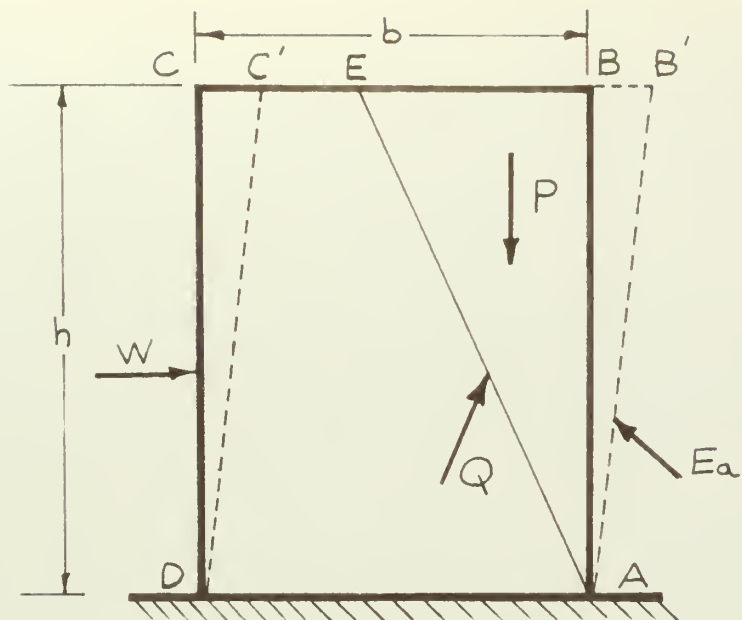


FIGURE VIII CELLULAR COFFERDAM ON ROCK

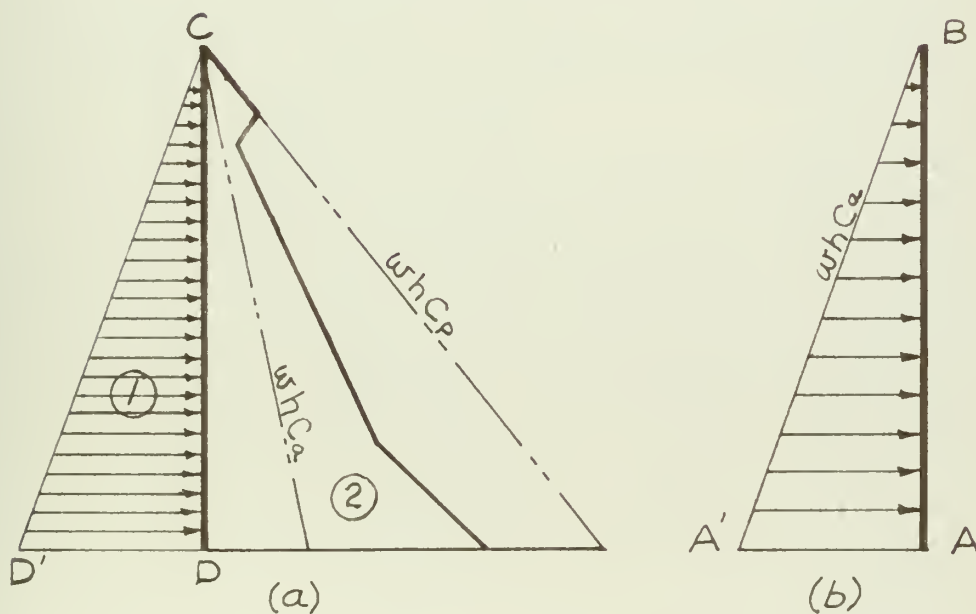


FIGURE IX PRESSURE DISTRIBUTION



misshapen under the effects of earth pressures at AB and external pressures at CD. Therefore the walls are distorted in a manner shown in Figure X. Figure XI (b) represents the active earth pressure distribution on wall AB, whereas Figure XI a represents the possible passive pressure distribution.

If the walls are considered to be flexible, we find that the active pressure distribution on the inner wall AB is no longer triangular because the deformation of the wall created pressure concentrations at the top and base of the wall.

By assuming that the resultant acting on the deformed wall AB has the same value as that which is found if a triangular distribution were used we find that

$$R_a = w \frac{h^2}{2} C_a \quad (13)$$

where

$$C_a = \tan^2 \left(45 - \frac{\phi}{2} \right)$$

As outlined in reference (21), a graphical solution reveals that the greatest pressure acting on wall AB occurs at the base and is equal to

$$p = w h C_a \quad (14)$$

The distribution of pressure on wall CD is considered in the following manner. External pressures deform the wall which moves against the earth fill material. Sheet pilings, have their own stiffness which is neglected. At equilibrium the sheet piles merely rest against the fill and are not stressed. When wall CD is flexed a thrust with a linear passive pressure occurs where as the deeper regions are influenced by the fact that the earth is confined within two walls which are comparatively close to each other.

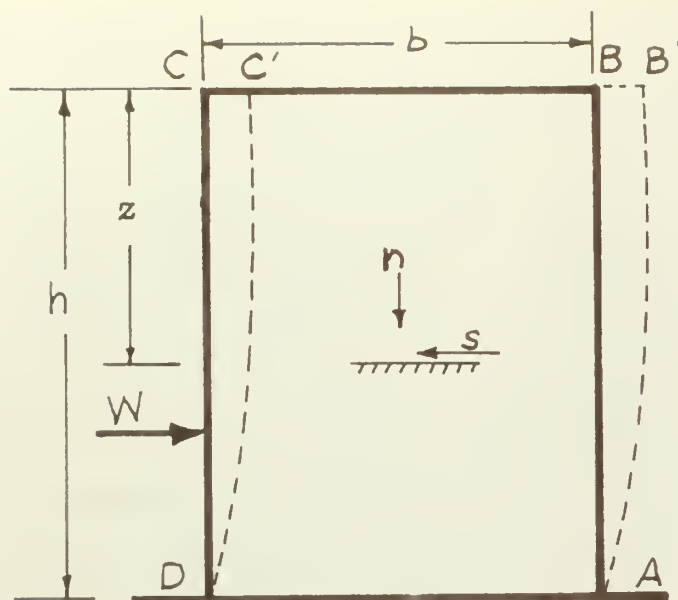


FIGURE X CELLULAR COFFERDAM ON ROCK (FLEXIBLE WALLS)

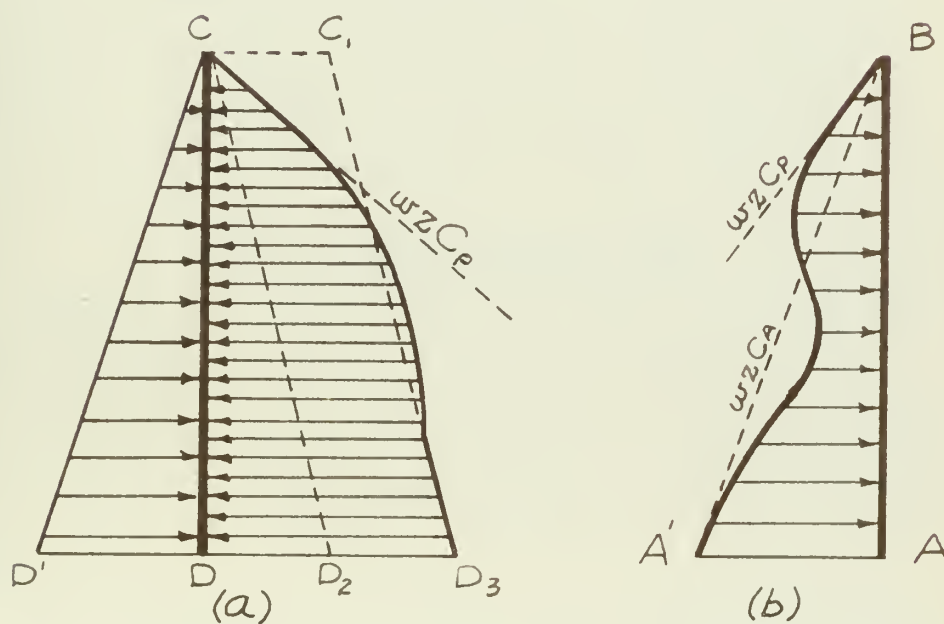


FIGURE XI PRESSURE DISTRIBUTION



If the deformation is sufficient, the slip planes which occur have a tendency to draw close to horizontal planes. At moment of slip Coulomb's relation for granular soils may be used. Thus

$$S = n \tan \phi \quad (15)$$

where S is the tangential pressure and n is the normal pressure as shown in Figure X. The angle of internal friction is represented by ϕ . Consider a horizontal plane at depth z and assume that the normal pressure due to the weight of the fill is uniformly distributed. This assumption is only true before external loads are applied. The resultant normal pressure is expressed by

$$n = wbz \quad (16)$$

where w - is the unit weight of the material. Therefore the resultant tangential pressure is

$$S = wbz \tan \phi \quad (17)$$

At the moment of load application, the smallest thrust existing against the wall is a active thrust. After loading and deformation have taken place, the tangential pressures come into action at z and the total resultant of pressures acting above z is

$$R_z = wbz \tan \phi + \frac{z^2}{2} \quad (18)$$

To find the pressures which give rise to these resultant pressures a graphical procedure is outline in reference (21).

A check must be made to see that this resultant is greater than the resultant W of the external pressures which is represented in Figure XI a.

If we substitute $z = h$ we can compute the total resultant pressure by using

$$R = wbh \tan \phi + w \frac{h^2}{2} C_a \quad (19)$$

The ratio $\frac{R}{W}$ shows the extent of safety obtained. If this ratio is given a value we are able to calculate the corresponding value of b , which is the effective width of the cofferdam.

Verdeyen in his conclusion emphasized that the calculations are approximate.

D. CONCEPTS BY S. PACKSHAW

A double wall cofferdam is constructed by driving the two longitudinal walls of piling in a straight line which are subsequently tied together by tie rods located near the top. The inner walls act as a simple vertical beam.

The earth pressure used in the design of the inner wall is derived from the formation of the unstable wedge AaB where Aa is the assumed failure line as shown in Figure XII. Inner wall pressure can be obtained from a triangle of forces consisting of the weight of the wedge W, the earth pressure P' , and the reaction Q along the failure plane. The earth pressure is equal to the active Rankine pressure when the angle of wall friction is zero.

Figure XIII represents the approximate distribution of pressure and resistance for a dam located on rock having relatively stiff walls.

The outer wall withstands an inward pressure due to the difference in water levels outside and inside the dam and is subject to tie rod load T imparted by the inner wall. To balance these forces earth resistance is developed by soil mass ADCa of Figure XII. This resistance is obtained by assuming that the unstable wedge AaB does not affect the resistance, except that force Q is considered as a super load applied to plane of rupture Aa. The soil above Aa is expanding whereas the soil to the left is contracting. An intermediate zone would contain the soil in an at rest condition.

For any point such as a or b the least resistance will be

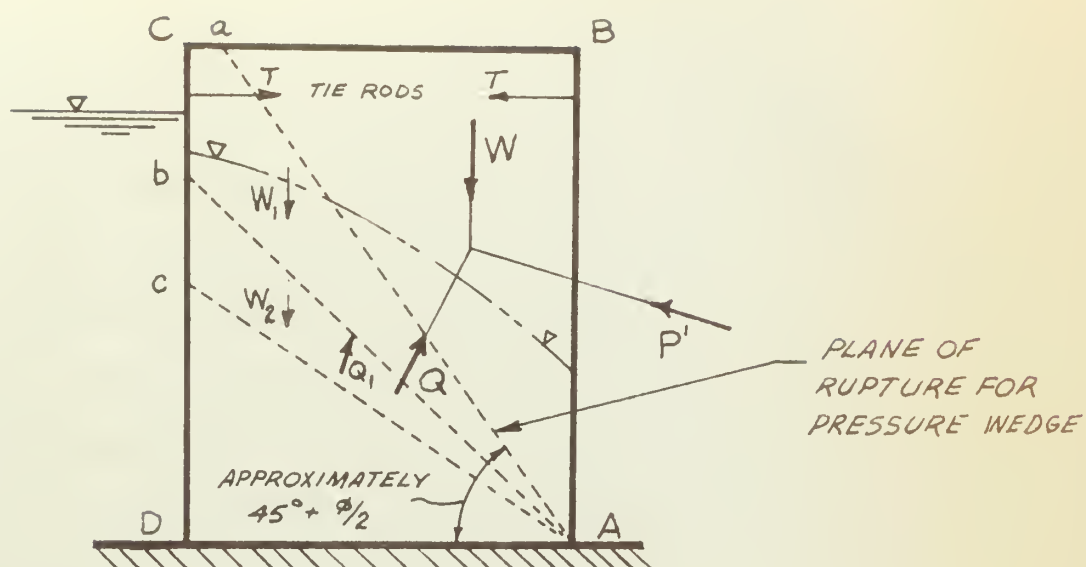


FIGURE XII RUPTURE PLANES FOR PRESSURE AND RESISTANCE

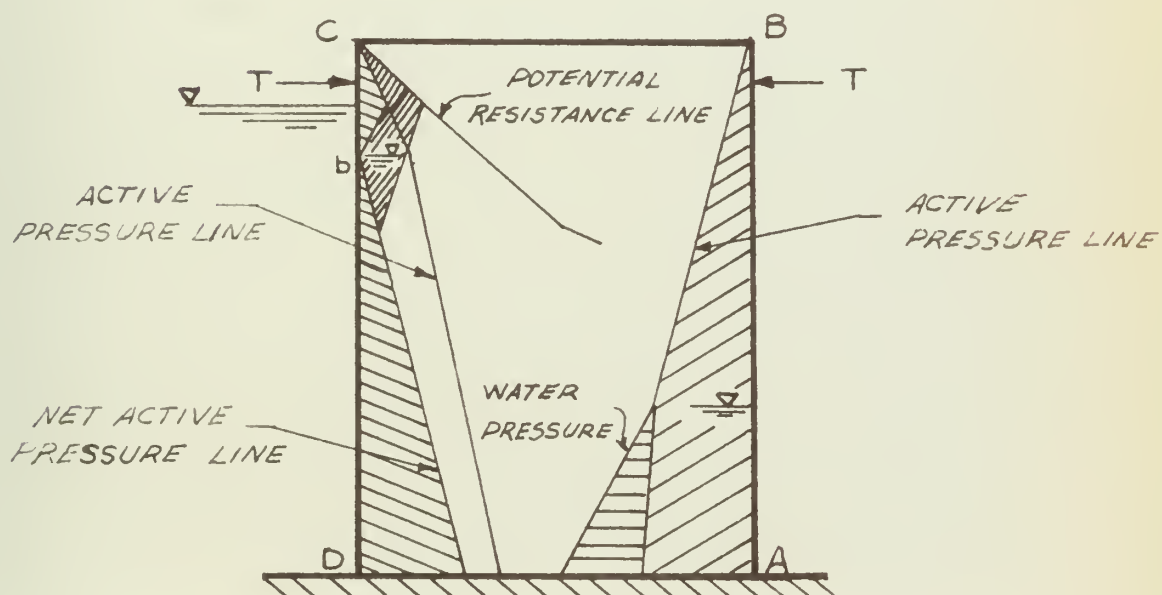


FIGURE XIII PRESSURE AND RESISTANCE DIAGRAM



developed by failure along a plane coinciding nearly with aA or bA respectively. By dividing the area $ADCa$ into a series of wedges radiating from A , equilibrium of forces for wedge $AbCa$ must be satisfied. The forces acting include the weight W_1 of the wedge, force Q from the pressure wedge, reaction Q_1 along bA and the earth resistance P_1 along bC . A polygon of forces can be drawn to determine the magnitude of the last two forces whose directions are known. The construction can be repeated for successive wedges so as to obtain the resistance due to each wedge. The potential resistance line, which shows the resistance that the soil can develop at narrow depths is indicated in Figure XIII.

A resistance line starts from point C or from intersection of failure line with outer wall. Usually very little resistance is developed in the upper quarter of the wall. Below that it increases rapidly. The least pressure on sheeting is the active earth pressure of the fill material. If a net diagram is used in design, it is found that the reaction at the upper support - that is, the tie rod load - does not exactly correspond to the full T from the inner wall. Probably the reaction at outer wall will be smaller than T , as a result the effect of the excess tie rod load will be to draw the wall in toward the fill and mobilize some of the potential resistance until the necessary increase in pressure behind the wall has been obtained, as shown by cross-hatched area in Figure XIII.

E. PHOTOELASTICITY

The science of photoelasticity is one of the main methods by which a complete exploration of maximum shears in a plane stress field can be determined with speed and accuracy. It provides a method whereby an entire stress field may be covered in one pattern.

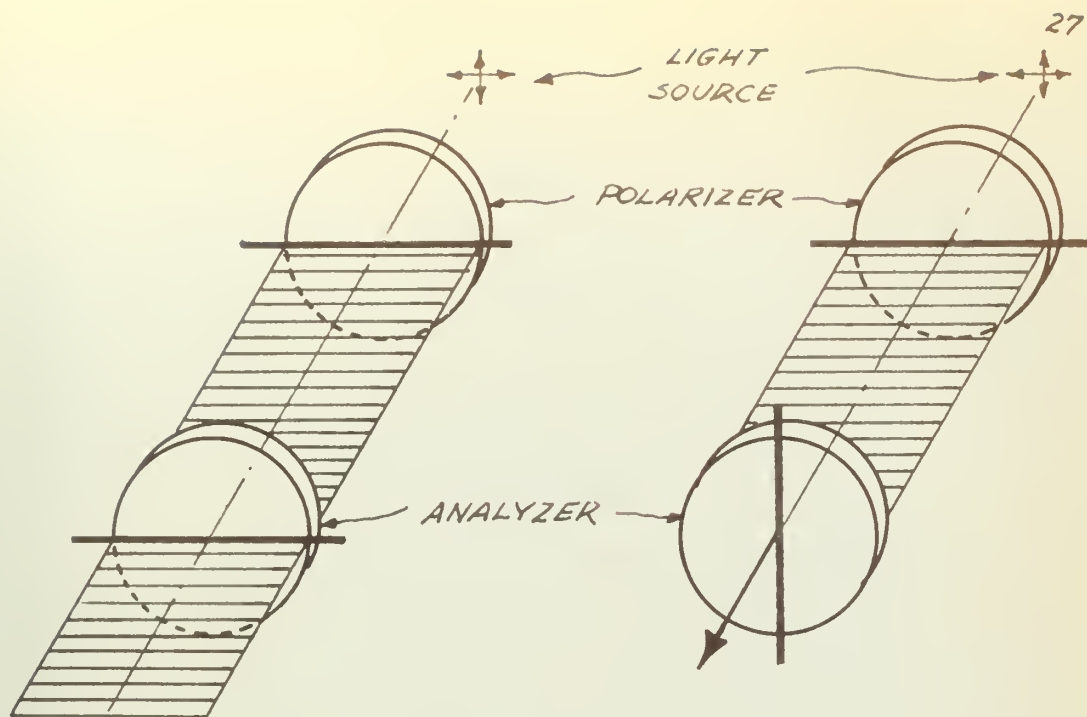
Photoelasticity is based on Brewster's Law which states that stress causes optically isotropic materials to become doubly refracting. If a transparent model is stressed in its plane and subjected to a normal polarized ray, this ray will be resolved into two component rays each vibrating in a plane of principal stress. These components travel at different velocities through the transparent medium. Therefore, the wave front of one wave travels ahead of the other by a small distance. If upon leaving the medium, the two components are combined to vibrate again in the same plane, interference takes place due to the relative displacement. The difference of principal stresses is directly proportional to the relative displacement and is also equal to twice the maximum shear at the line of passage. This difference of principal stresses changes continuously from point to point. As a result, optical displacements will also change and isochromatic bands will form. These isochromatic lines indicate points of equal maximum shear.

By measuring the positions of planes of polarization and their difference, it is possible to compute the principal stresses at every point in the model.

Figure XIV is a graphical representation of the essential

elements and optical transformations that occur in a plane polariscope. A schematic diagram of the circular polariscope is shown in Figure XV.

For a detailed description of photoelasticity the reader is referred to reference (10).



(a) PARALLEL

(b) CROSSED

FIGURE XIV PLANE POLARISCOPE

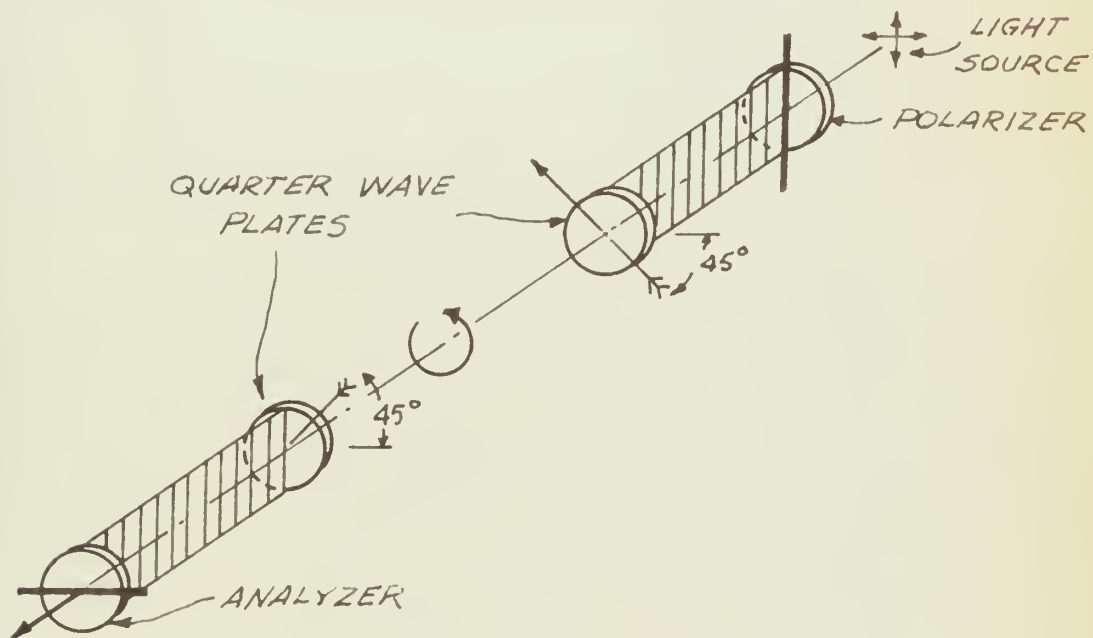


FIGURE XV CIRCULAR POLARISCOPE

PART III

APPARATUS

Since the thesis was of a basic research type, the apparatus used was gradually developed through a trial and error process. Modifications were made as each test was conducted, and are explained in detail in other parts of this thesis.

A. POLARISCOPE

At the outset of the investigation a standard General Radio Company Polariscope, TYPE No. 1534-A, serial Number 104 was used. The light source contained a 100 watt bulb which was located behind a light diffuser type 1534-P2. Circular 10 inch polarizer and analyzer type 1534-P, with gradations from 0° to 90° were mounted on frames which could be moved along two rails and clamped in any desired location. A green filter type 1534-P5 was located between the diffuser and the polarizer. The completely assembled polariscope is shown in Figure XVI.

B. LOAD APPLICATION DEVICE

This consisted of a Soil Test Machine, Model D-110, made by Soil Testing Services, Evanston, Illinois. The equipment was slightly modified to provide a tensile load rather than a compressive force. It consisted of a differential pulley mounted on a shaft which in turn was connected to a set of worm gears. Through these worm gears the loading shaft could be made to advance or retract. The shaft was in turn connected to a 100 pound proving ring on which a dial was mounted. A sleeve containing two set screws was



Figure XV I ELEMENTS OF THE POLARISCOPE

(A) Analyzer, (B) Polarizer, (C) Filter, (D) Light source with diffuser.

mounted on the shaft. A 2 inch steel spacer strip was screwed into place on the other end of the sleeve. The spacer contained two $1/16$ " holes through which two steel rods were inserted. The rods were threaded at their extremities and two nuts were provided for each end. The opposite end of rods contained an aluminum spacer strip which contained a pointed screw in the center. This pointed screw was inserted in a hole punched in the vertical member of the model at the desired point of application. This set up permitted the load to be applied at any elevation from the bottom of the model to the top.

Motor The power was supplied by a geared down Delco Motor Model A2120, which was rewound in order to incorporate a reversing switch so that the load could be stopped at any desired instant. The load application device is shown in Figure XVII.

C. MODELS

For preliminary investigations a wooden model, consisting of a 2" x 18" base and two 2" x 4" x 12" vertical walls connected to the base by strap hinges, was used. This wooden model was used to test the feasibility of the project and also to select the most sensitive photoelastic materials.

A steel model constructed of $\frac{1}{4}$ " x $1\frac{1}{2}$ " steel was used during the experiment. Two vertical 12" strips were connected to a 18" base by means of strap hinges which were brazed to the vertical walls and base piece respectively. One hinge was placed on the inside and the other was placed on the outside. Two aluminum

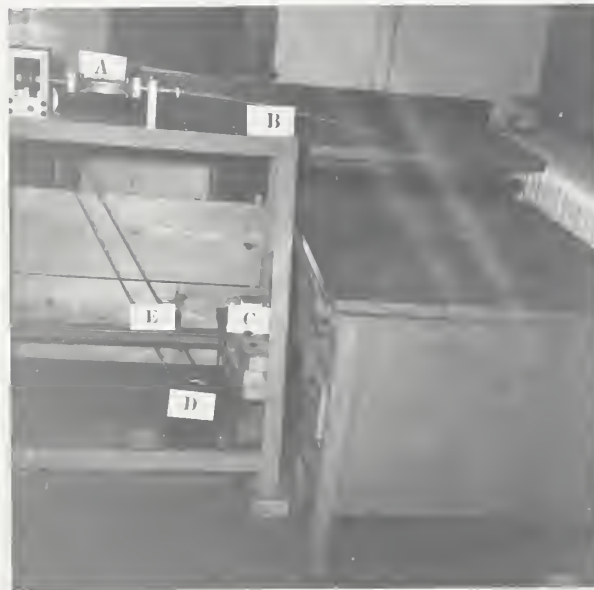


Figure XVII LOADING DEVICE

(A) Proving ring, (B) Steel extension rods (C)
Reversing switch, (D) Motor, (E) Frame and pulley
belt.



Figure XVIII COFFERDAM MODELS

(A) Wooden model with assorted cylinders

(B) Steel model with epoxy resin cylinders.

strips were used to tie the vertical members at the top. These strips were placed in such a manner that the sides of the model could move freely. The inside dimensions of the model were $9 \frac{3}{4}$ inches by $11 \frac{1}{2}$ inches. Both types of models are shown in Figure XVIII.

D. PHOTOGRAPHIC EQUIPMENT

Camera A Auto Graflex, curtain aperture camera with a f 13.5 cm lens and modified for 120 roll film was used.

Film The film used was Kodak TRI-X-120 roll film.

Subsequent tests revealed that the light source was not sufficient. This was corrected by removing the light source located on the polariscope and using a Delineascope Model D, Number 47314. The completely assembled apparatus is shown in Figure XIX.

E. MATERIALS

The photoelastic material used during the investigation was the epoxy resin 6000A, manufactured by Houghton Laboratories, Olean, New York. Technical data and specifications for the material are found in the Appendix.

The $\frac{1}{4}$ inch rods were received in 3 foot lengths. These in turn were cut on a steel band saw to $13/16$ inch lengths, and subsequently turned to $.750 \pm .002$ inches on a lathe. Machining processes were accomplished as recommended by the manufacturer. Approximately 189 feet of rod were cut and used during the experiment. An attempt was made to order various diameter sizes ranging from $1/8$ inch to $1/4$ inch. However, the delay in shipment and excessive costs prevented the use of these smaller sizes. The $1/4$ inch diameter rod was the smallest standard size available.

PART IV

METHOD OF PROCEDURE

Since the investigation was basic in nature, many initial problems encountered required trial and error solutions. Therefore, the procedure is subdivided into a preliminary phase and a final phase. The preliminary phase deals with the initial problems and the methods used to overcome these problems. Considerations in the final phase will include the technique and procedure used, as developed in the preliminary phase, from which the results of the investigation have been determined.

A. PRELIMINARY PHASE

The main objective of the preliminary phase was to:

1. Select the photoelastic material to be used.
2. Devise the most suitable apparatus.
3. Determine the required aperture opening and time exposure for sharp and distinct photographs.
4. Most efficient arrangement of the polariscope.
5. Improved developing and printing technique.

A wooden model, as described previously, was used for the purpose of selecting the most sensitive photoelastic material. Small cylinders of lucite, marbolite and epoxy resin were used. These were stacked in the model and wooden cylinders of assorted sizes were used as a filler material. The photoelastic cylinders were coated with a light coat of mineral oil. A lateral load was applied and the model was observed in a polarized field. This

simple test revealed distinct stress patterns within the epoxy resin which altered as the load was slightly changed. As a result the epoxy resin was selected for use in the investigation.

The loading device described in the "Apparatus" section was used throughout the investigation. Calibration of the proving ring was done with a spring balance and the calibration curve is shown in Figure XXX.

At this stage of the investigation, the steel model was used. In stacking the epoxy resin cylinders within the model, it was noticed that an integral number of cylinders could not be placed adjacent to each other. This necessitated the placement of a $\frac{1}{4}$ " steel strip on the inside of the loaded wall and fastened to it by $\frac{1}{4}$ inch flat head, countersunk screws. To present a horizontal surface at the base a similar strip was placed and fastened as described above. This was done to eliminate the uneven surface caused by the hinge placed on the inside of the model. This modified arrangement permitted the placement of 38 cylinders aligned in a row adjacent to each other across the width of the model. The new inside height of the model was $11\frac{1}{2}$ inches.

Photographing techniques were accomplished by loading the model and taking photographs at various lens openings and time exposures. Contact prints revealed that a lens opening of f 4.5 with a time exposure of 1 second produced sharp and distinct photographs.

To obtain the best arrangement of the polariscope a

similar procedure was used and the following polariscope combinations were used;

1. Crossed and parallel plane polariscope using a white light source.
2. Crossed and parallel plane polariscope using a green filter which provided monochromatic light.
3. Standard crossed circular polariscope.
4. Circular polariscope with various orientations of the quarter wave plates.

As a result of these tests, the standard crossed plane polariscope was selected. It produced sharp and distinct stress patterns. This arrangement was used throughout the investigation.

At this stage of the investigation it was observed that the light intensity was not uniform and that the stress patterns were distinct within a circular zone 2 inches in diameter only. Portions outside this zone were blurred. To rectify this condition the back portion of the diffuser was removed and a dilencoscope, together with a 5 inch convex lens with a focal length of 10 inches, was incorporated in the apparatus. This arrangement increased the range of uniform light intensity to a 5 inch circle, but simultaneously decreased the sharpness of stress patterns in that the rays of light were not parallel.

During this preliminary phase it was also observed that the ends of the cylinders became cloudy after a period of about 10 minutes. Because the time element prevented the polishing

of the ends, the writer decided to lightly brush the ends of the cylinders, with an ox hair brush, immediately prior to the taking of a photograph. Although this procedure minimized the condition it was very inconvenient.

B. FINAL PHASE

The arrangement shown in Figure XIX proved to be the most effective for the equipment available and the limited time available for conducting the investigation.

Final tests were conducted in the following manner:

1. Cylinders were placed individually within the model, in layers, to a height of 2 inches below the top of the model.
2. Glass plates and a level were used to align the cylinders so that the ends were located in vertical planes.
3. An atomizer was used to coat the ends of the cylinders with oil. A combination of halowax and mineral oil produced an index of refraction similar to the cylinders. To provide a minimum coat of oil and uniform distribution, the atomizer was used at a distance of 1 foot from the model.
4. The model was then placed on a wooden block and clamped in place. In preliminary testing the base of the model near the loaded wall was raised as the lateral load was applied. This condition was rectified by clamping the model with C-clamp to the wooden block.



Figure XIX FULL VIEW OF EXPERIMENTAL SETUP

(A) Dolineascope, (B) Convex lens, (C) Extensometer dial attached to polariscope, (D) Steel model, (E) Loading device, (F) Reversible switch (G) Camera.

5. A extensometer dial was placed at the $\frac{1}{4}$ point of the unloaded wall. This dial recorded the horizontal displacement of the wall.
6. Prior to the application of the load the entire apparatus was checked in both the vertical and horizontal directions to ascertain that the equipment was level and that the ray of light was normal to the cylinders.
7. A photograph was taken of the model in an unloaded state. The initial reading, on the loading ring and extensometer dial, was recorded.
8. The motor was started and the load was applied for a period of two minutes. At this point the motor was stopped and readings of the loading ring and extensometer dial were recorded. A photograph was taken and the load was again applied for an additional 2 minute period at which time the process was repeated until failure occurred.

Tests were conducted for the following arrangements.

1. Cylinders placed in a dense condition.
2. Cylinders placed in a loose condition.

To achieve uniformity in the results the cylinders were removed, wiped dry and replaced in the model after each test. This task proved to be tedious and time consuming. Extreme caution had to be utilized when loading the cylinders in the loose state.

A slight disturbance would collapse the structural arrangement and necessitate the removal of the cylinders and repeating the loading procedure. This condition was eliminated by clamping the unloaded wall to the base with a c-clamp.

C. DEVELOPING PROCEDURE

The exposed TRI-X film was developed in a Kodak tank using Microdal solution. Initial rolls were developed in a period of 15 minutes. Developing time was increased 3 minutes for every additional 4 rolls processed. Washing time was 30 seconds in ordinary tap water. Kodak acid fixer, prepared as recommended by the manufacturer, was used to fix the film. The time of fixing was one-half the developing time and not exceeding a maximum of 10 minutes. Finally, the film was washed in running tap water, for a period of 15 to 20 minutes. The film was wiped and permitted to dry overnight.

D. PRINTING PROCEDURE

Contact prints were made by exposing the negative to Kodak, Resisto N-2 photographic paper in a printer. A 4 second exposure produced the desired results. The print was then immersed in Dektal solution for an average time of 45 seconds. It was then suspended in a 28 percent acetic acid bath for 30 seconds. Final fixing was accomplished in a Kodak acid fixer solution for a period of 10 minutes. After washing in a print washer for 20 minutes, the prints were removed and dried with blotters. Final drying was accomplished by using a ROTO photo print dryer.

PART V

RESULTS AND DISCUSSION

The purpose of this portion of the study is to describe in detail the results obtained. Difficulties encountered with the apparatus and the subsequent modifications have been discussed previously. Therefore, this section will be primarily concerned with the photographic results obtained in five tests.

Results are presented in the form of a continuous series of photographs taken at various time intervals and a load versus yield curve. A detailed discussion follows the results for each test.

TEST I

This test was conducted with the apparatus arranged as shown in Figure XIX, except that the original light source mounted on the polariscope was used. The cylinders were stacked in a dense state - that is - each cylinder had six contact points. The model contained 1350 cylinders.

Preliminary tests revealed that most of the internal activity occurred in a zone which extended from the center of the model to the unloaded wall. As a result the photographs were taken to include the unloaded wall as the left boundary, the base as the lower boundary and cover approximately 70 percent of the model. The photographs are shown in Figure XX.

The testing procedure outlined previously was used and the tabulated readings are shown in the Appendix.

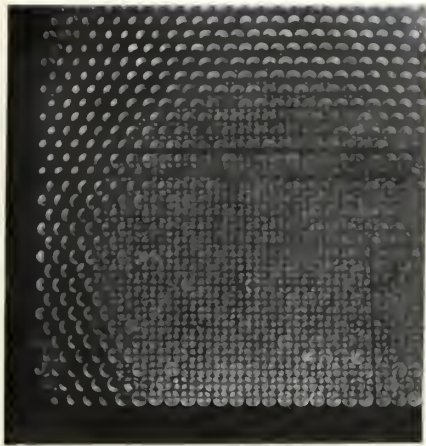


Figure XX a

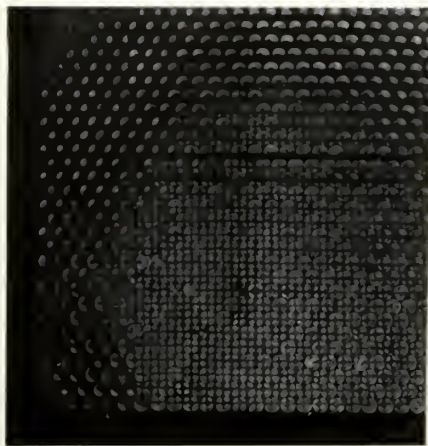


Figure XX b

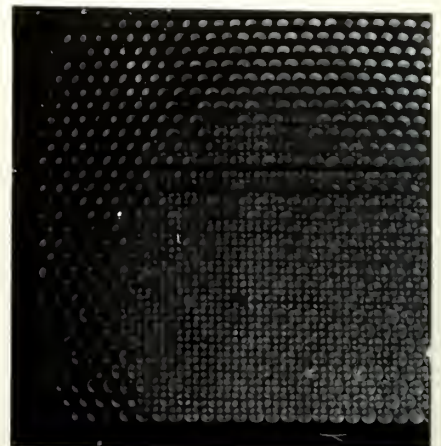


Figure XX c

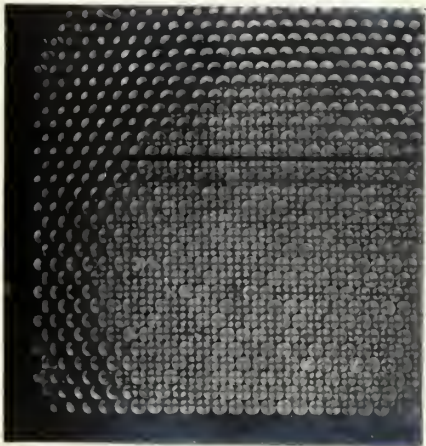


Figure XX d

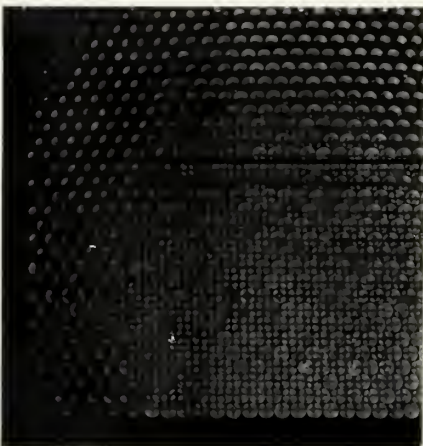


Figure XX e

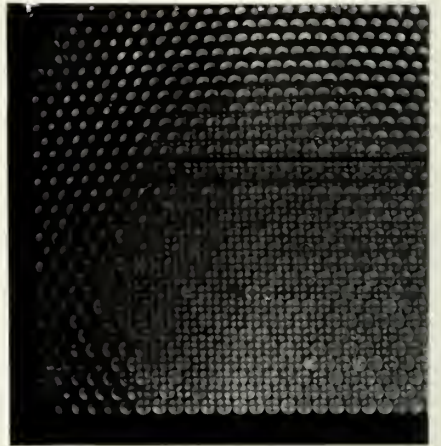


Figure XX f

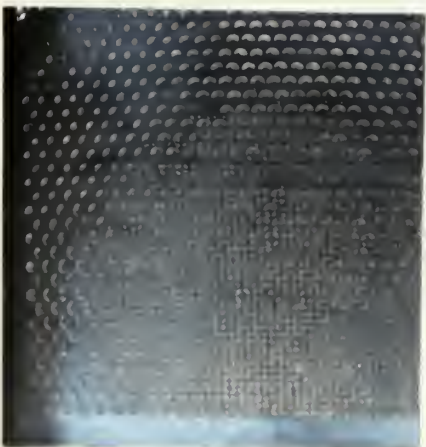


Figure XX g

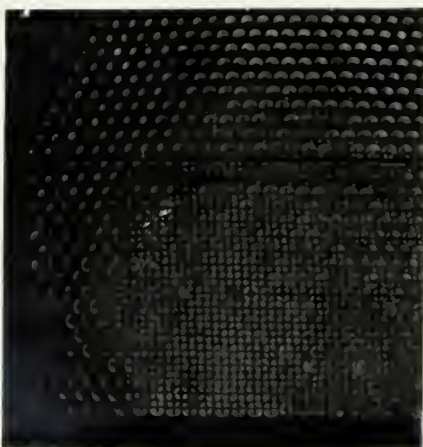


Figure XX h



Figure XX i

Figure XX PHOTOGRAPHIC RESULTS -- TEST 1

Figure XX a No load condition with residual stress patterns in the cylinders.

Load = 0.0 Lbs. Yield = 0.0 %

Figure XX b Load = 0.8 Lbs. Yield = 0.6 %

Figure XX c Slight "wave" begins to form in central portion near the horizontal reference line.

Load = 0.9 Lbs. Yield = 1.2 %

Figure XX d "Wave" crest increases in a vertical direction.

Load = 1.0 Lbs. Yield = 1.9 %

Figure XX e "Wave" extends in a horizontal direction.

Load = 1.3 Lbs. Yield = 2.6 %

Figure XX f Wave action increases and extends below the horizontal reference line,

Load = 1.0 Lbs. Yield = 3.3 %

Figure XX g Cylinders in lower right portion begin to displace toward the left.

Load = 1.0 Lbs. Yield = 4.1 %

Figure XX h Extensive arching in central portion

Load = 1.3 Lbs. Yield = 4.8 %

Figure XX i Arching increases in both directions - that is - above and below the horizontal reference line

Load = 1.3 Lbs. Yield = 5.5 %

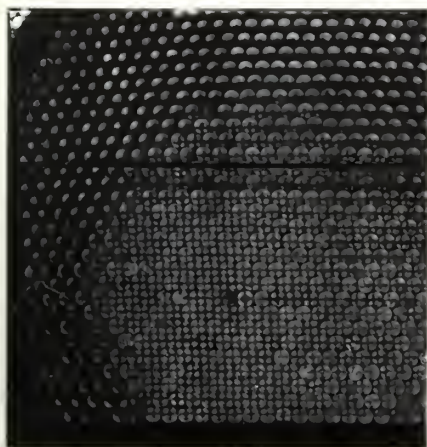


Figure XX j

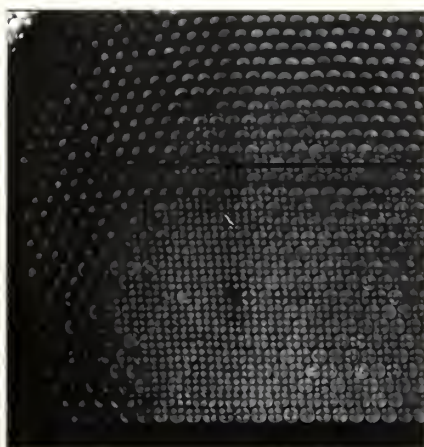


Figure XX k



Figure XX l

Figure XX PHOTOGRAPHIC RESULTS. -- TEST I (CONTINUED)

Figure XX j Noticeable movement of cylinders in the lower right portion of the model.

Load = 1.4 Lbs.

Yield = 6.2 %

Figure XX k Failure planes appear at an angle of 65° with the horizontal base. Extensive movement of cylinders in the lower right section of the photograph.

Load = 1.7 Lbs.

Yield = 8.3 %

Figure XX l Distinct failure plane appears at an angle of 65° with the horizontal and passing through the center of the "Wave". Horizontal failure planes appear in the lower right hand portion.

Load = 1.5 Lbs.

Yield = 10.2 %

DISCUSSION

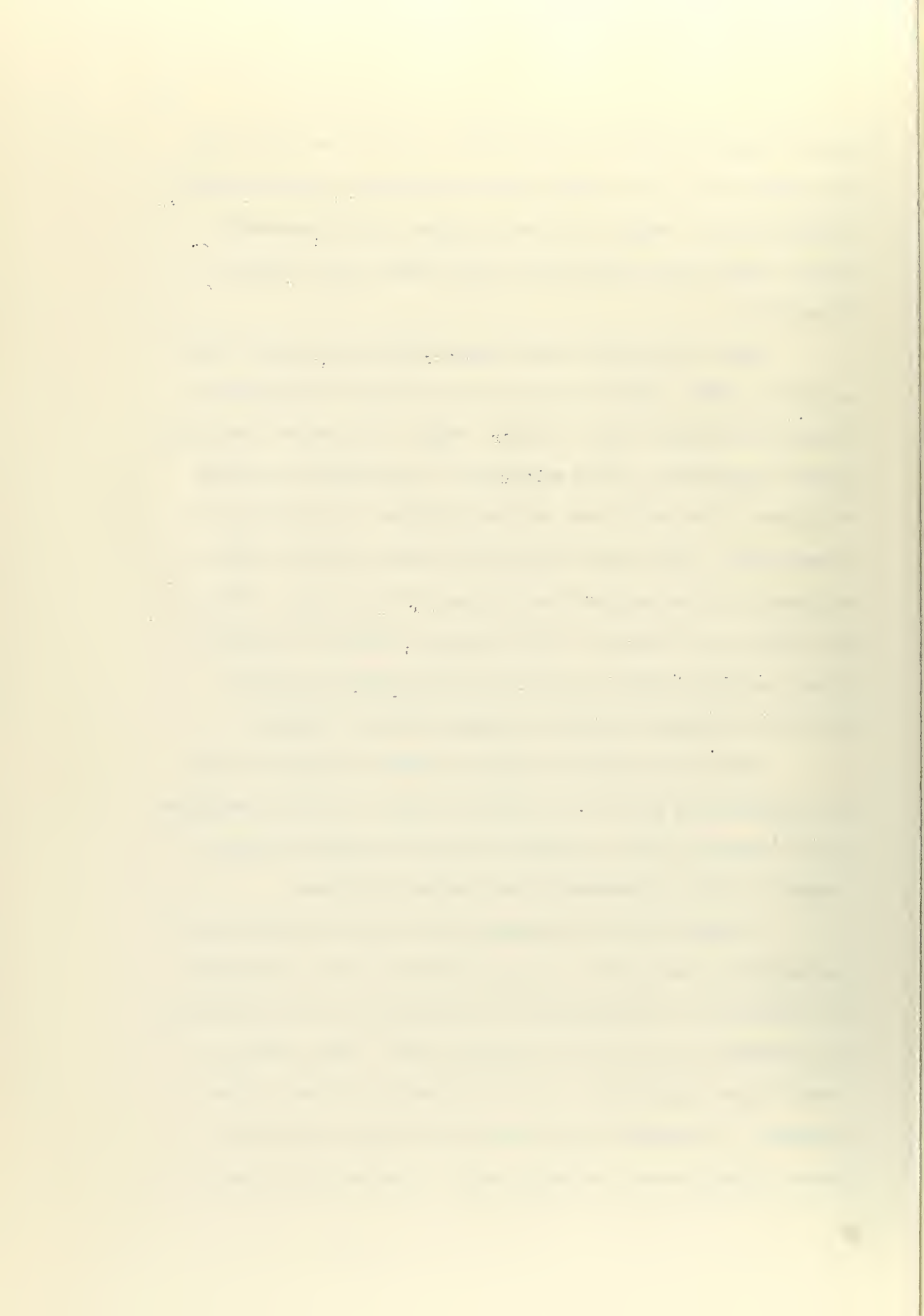
As the load increased it was observed that the arching effect began in the center of the model in the vicinity of the horizontal reference line. This reference line is the steel rod used to apply the load at the $1/3$ point above the base. The arching

effect progressed upward to the surface. As the load approached the maximum value, the arching zone extended below this horizontal reference line. Finally the arch collapsed and a pronounced failure plane formed through the crest of the arch as shown in Figure XX 1.

This test revealed that three distinct zones were formed within the model. Zone one was in the vicinity of the unloaded wall, and was shaped in the form of a wedge. It appeared that this entire zone moved as a unit and dropped in a downward direction at failure. The second zone was characterized in the form of a curved sector. This zone contained the central portion of the collapsed arch and included the distinct failure plane. Finally the zone in the vicinity of the loaded wall contained cylinders which, displaced toward the left by rolling over each other, this zone contained noticeable horizontal failure surfaces.

Figure XXI shows the relation between the applied load and corresponding yield. The scattered points are partly explained by the relaxation which occurred when the load application was stopped in order to photograph the internal structure.

A limited field of uniform light intensity and the use of non-homogeneous material is clearly indicated in the photograph. The difference in the sharpness of the internal stress patterns of the cylinders is due to the "clouding" effect. This effect is caused by the evaporation of the oil placed on the ends of the cylinders. To minimize this effect some of the cylinders were brushed lightly with an ox hair brush. By polishing the ends of



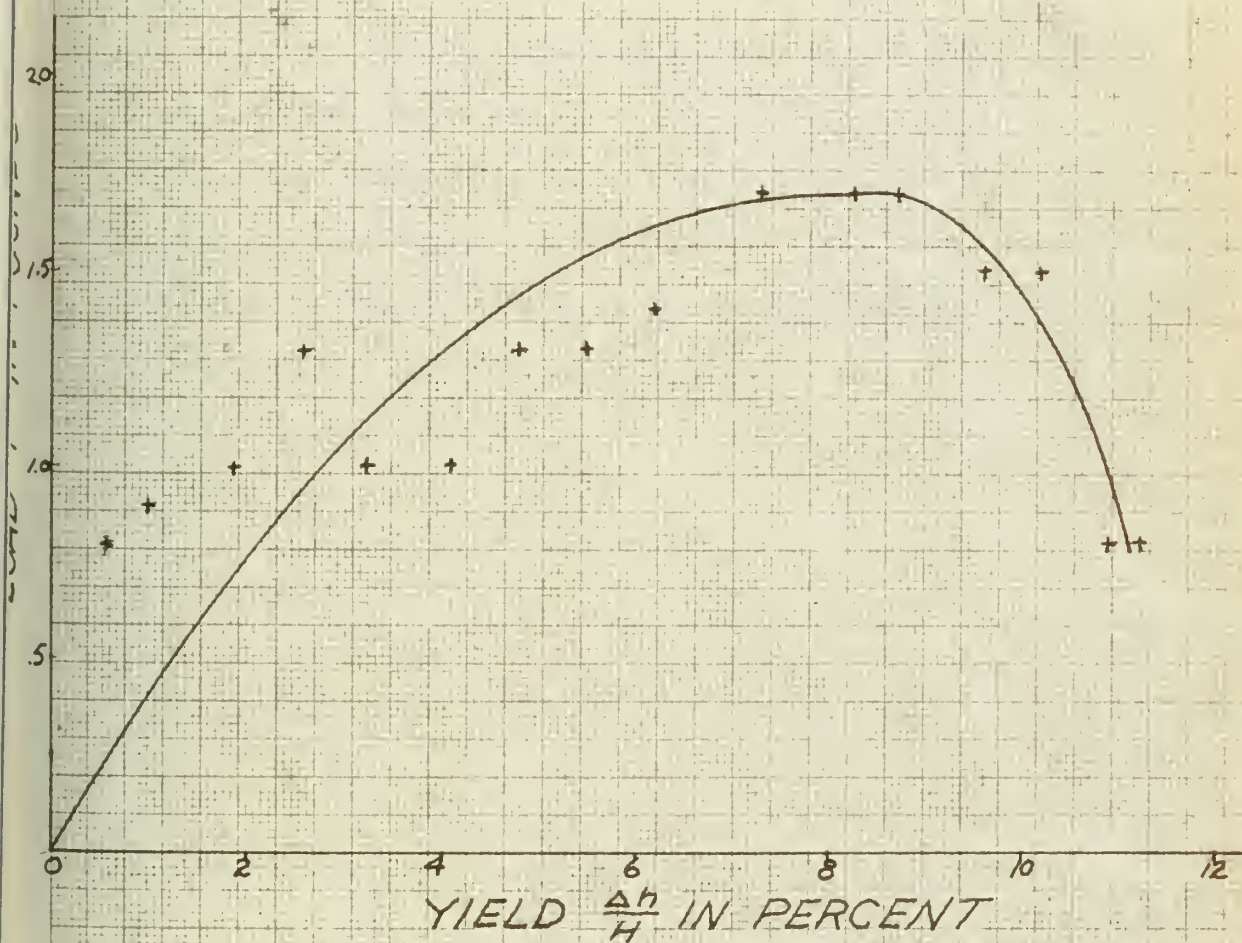
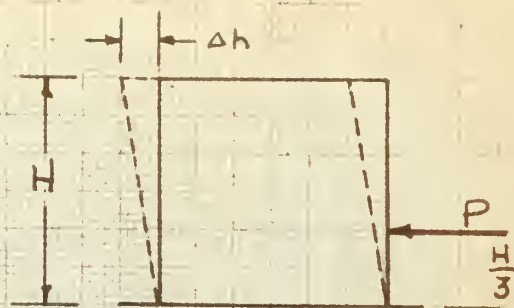


FIGURE XXI LOAD AND YIELD CURVE (TEST # 1)

the cylinders, this effect can be completely eliminated.

Eccentric stress patterns at the periphery of the illuminated area are caused by light rays entering the cylinders at an oblique angle of incidence.

Close observation of the photographs will show that the stress patterns within the cylinders are changed in highly stressed areas. This indicates that there is a possibility of actually computing the stresses at point contacts in the vicinity of the failure plane.

At failure, the cylinders at the surface of the model were similar, in position, to those shown in Figure XX 1. However, the cylinders in the immediate vicinity of the loaded wall were displaced upward about .25 inches from their original horizontal position. This is obviously due to the frictional forces between the cylinders and steel vertical wall.

TEST 2

This test was conducted by using the same procedure outlined in test 1, with the following modifications.

1. A delineascope was used to increase the intensity of the light source.
2. Light rays were concentrated by placing a 5 inch convex lens between the light source and diffuser.
3. The base of the model was not restrained by a C.-clamp.
4. Cylinders were stacked to a height of 2 inches below the crest of the model. This arrangement contained 1650 cylinders as compared to 1350 cylinders used in test 1.
5. Photographs were taken at 3 minute intervals.

Photographic results of this test are shown in Figure XXII. Tabulated raw data are contained in the Appendix.

1. The first part of the paper is devoted to the study of the properties of the function $f(x)$ defined by the equation $f(x) = \int_0^x f(t) dt$. It is shown that $f(x)$ is a constant function, and its value is determined by the initial condition $f(0) = 1$.

2. In the second part, we consider the function $g(x)$ defined by the equation $g(x) = \int_0^x g(t) dt$. It is shown that $g(x)$ is a constant function, and its value is determined by the initial condition $g(0) = 1$.

3. The third part of the paper is devoted to the study of the properties of the function $h(x)$ defined by the equation $h(x) = \int_0^x h(t) dt$. It is shown that $h(x)$ is a constant function, and its value is determined by the initial condition $h(0) = 1$.

4. In the fourth part, we consider the function $k(x)$ defined by the equation $k(x) = \int_0^x k(t) dt$. It is shown that $k(x)$ is a constant function, and its value is determined by the initial condition $k(0) = 1$.

5. The fifth part of the paper is devoted to the study of the properties of the function $l(x)$ defined by the equation $l(x) = \int_0^x l(t) dt$. It is shown that $l(x)$ is a constant function, and its value is determined by the initial condition $l(0) = 1$.

6. In the sixth part, we consider the function $m(x)$ defined by the equation $m(x) = \int_0^x m(t) dt$. It is shown that $m(x)$ is a constant function, and its value is determined by the initial condition $m(0) = 1$.

7. The seventh part of the paper is devoted to the study of the properties of the function $n(x)$ defined by the equation $n(x) = \int_0^x n(t) dt$. It is shown that $n(x)$ is a constant function, and its value is determined by the initial condition $n(0) = 1$.

8. In the eighth part, we consider the function $o(x)$ defined by the equation $o(x) = \int_0^x o(t) dt$. It is shown that $o(x)$ is a constant function, and its value is determined by the initial condition $o(0) = 1$.

9. The ninth part of the paper is devoted to the study of the properties of the function $p(x)$ defined by the equation $p(x) = \int_0^x p(t) dt$. It is shown that $p(x)$ is a constant function, and its value is determined by the initial condition $p(0) = 1$.

10. In the tenth part, we consider the function $q(x)$ defined by the equation $q(x) = \int_0^x q(t) dt$. It is shown that $q(x)$ is a constant function, and its value is determined by the initial condition $q(0) = 1$.

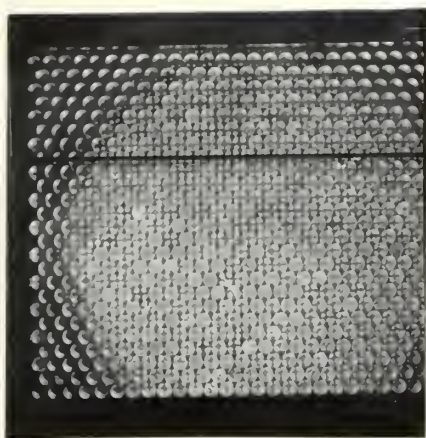


Figure XXII a

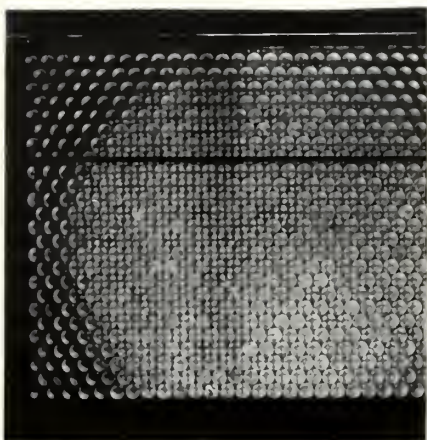


Figure XXII b

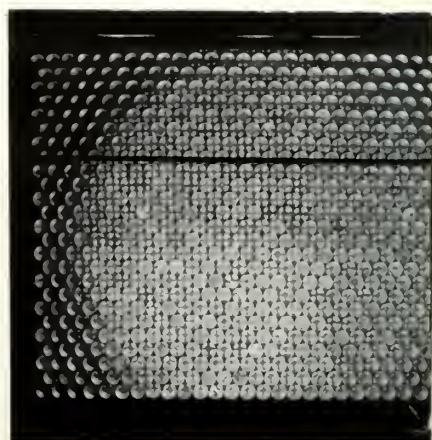


Figure XXII c

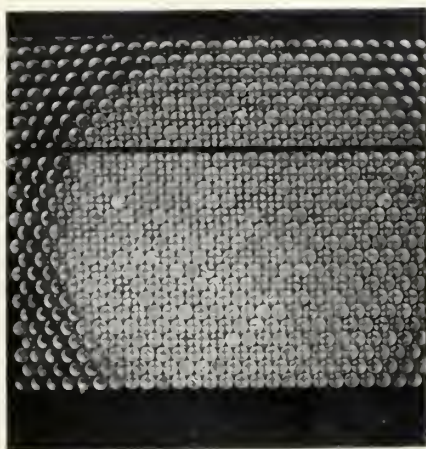


Figure XXII d

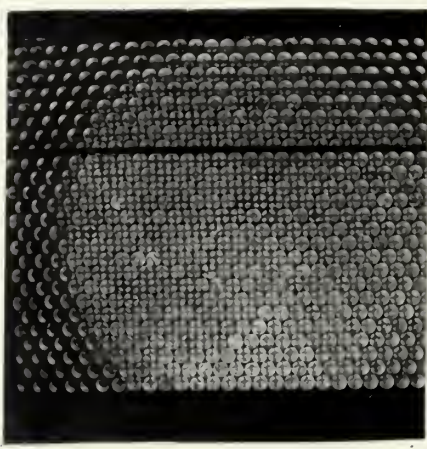


Figure XXII e

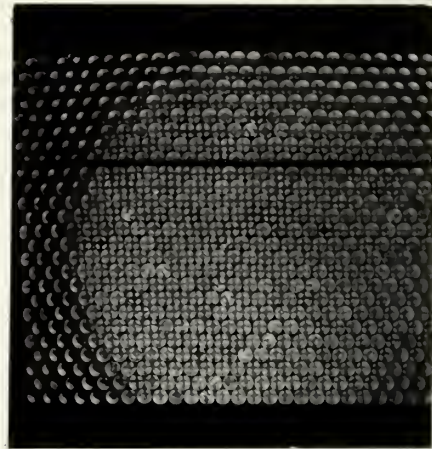


Figure XXII f

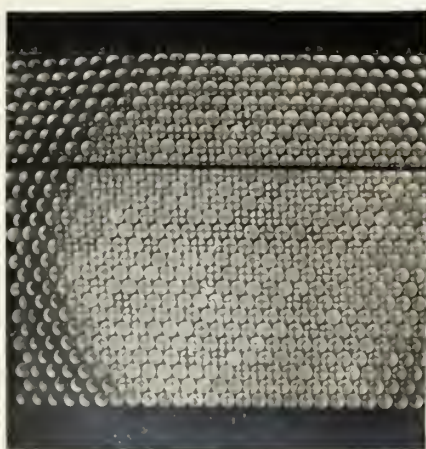


Figure XXII g

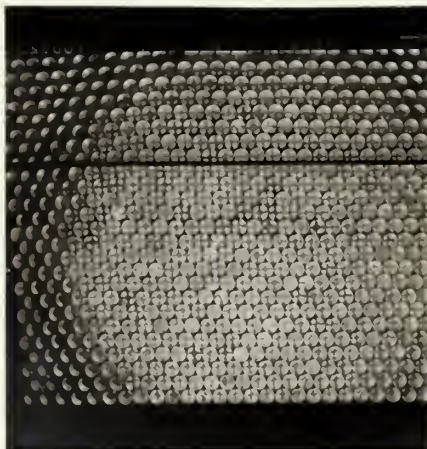


Figure XXII h

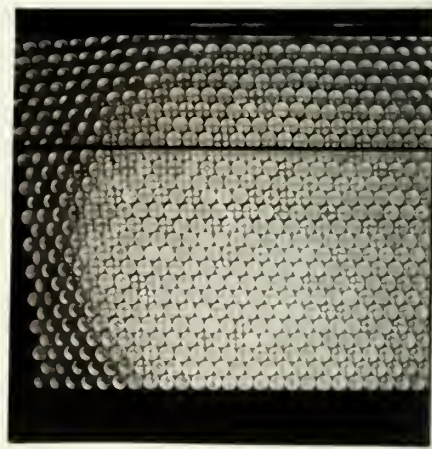


Figure XXII i

Figure XXII PHOTOGRAPHIC RESULTS -- TEST 2

- Figure XXII a No load condition with residual stresses in the cylinders.
- Load = 0.0 Lbs. Yield = 0.0 %
- Figure XXII b Load = 0.9 Lbs. Yield = 0.9 %
- Figure XXII c Slight arching in central portion near horizontal reference line.
- Load = 1.0 Lbs. Yield = 1.9 %
- Figure XXII d Progressive arching in vertical direction above horizontal reference line.
- Load = 1.4 Lbs. Yield = 3.0 %
- Figure XXII e Arching extends below horizontal reference line. Lower right cylinders begin lateral displacement to the left.
- Load = 1.7 Lbs. Yield = 4.0 %
- Figure XXII f Noticeable "wave" action in central portion. Extensive lateral displacement of cylinders occurring in left center portion.
- Load = 1.8 Lbs. Yield = 5.2 %
- Figure XXII g Wave action increases. Failure planes appear in central portion making an angle of approximately 63° with the horizontal.
- Load = 2.2 Lbs. Yield = 6.2 %
- Figure XXII h Additional wave crest forms near unloaded wall. Extensive separation of cylinders near central portion.
- Load = 2.4 Lbs. Yield = 7.4 %
- Figure XXII i Failure plane passing through the peak of the initial "wave" crest is visible.
- Load = 2.1 Lbs. Yield = 8.0 %

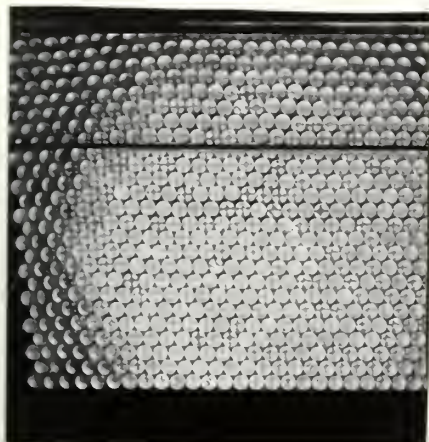


Figure XXII j

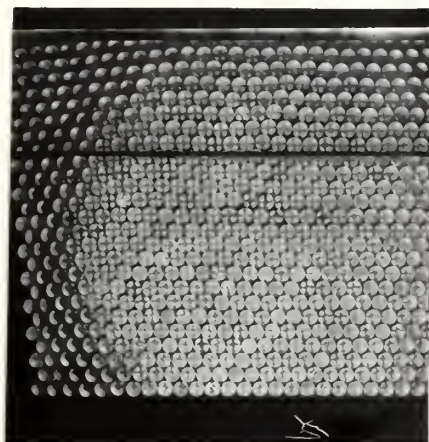


Figure XXII k

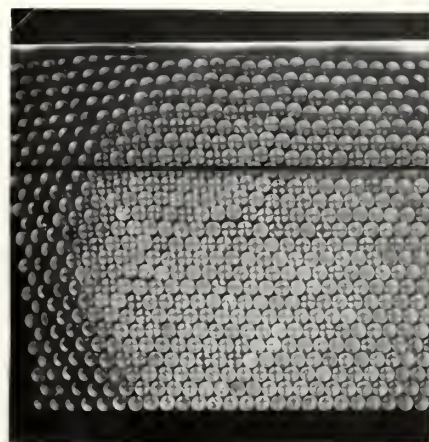


Figure XXII l

Figure XXII PHOTOGRAPHIC RESULTS - TEST 2 (CONTINUED)

Figures XXII j and k Formation of visible failure plane through the second "wave" crest.

Load = 1.8 Lbs.

Yield = 8.9 %

Figure XXII l Distinct failure planes passing through the centers of both "wave" crests at an angle of approximately 66° with the base. Horizontal failure planes are visible in the central portion.

Load = 1.0 Lbs.

Yield = 10.6 %

DISCUSSION

During the initial stages of the test the effects were similar to those observed in the previous test. However, an additional wave crest was formed near the unloaded wall when the load was at its maximum value of 2.4 pounds and a corresponding yield of 7.4 %.

Three distinct zones of activity also appeared in this test. These zones are more clearly visible as a result of the increased intensity of light used. However, the stress patterns

within the cylinders are not as distinct and centered as those of Test 1. This is explained by the fact that the light rays were not statistically parallel. Although the lens produced more illumination it was detrimental in that it produced rays which are not parallel when they strike the diffuser. This effect can be minimized by using a more effective diffuser.

The load versus yield curve, as shown in Figure XXIII, contains a steeper slope and a minimized relaxation effect.

A comparison of this curve with that of the previous test indicates that the former contains a maximum ordinate of 2.4 pounds and the latter a ordinate of 1.7 pounds. The yield values are similar.

During the test it was noticed that the right side of the base of the model raised to a maximum height of .5 inches. The clouding effect, as shown in Figure XXII was also present.

A increase in the number of cylinders required a greater load for failure although the yield in both tests was approximately 11 percent.

The maximum load in both tests was reached in 21 minutes.

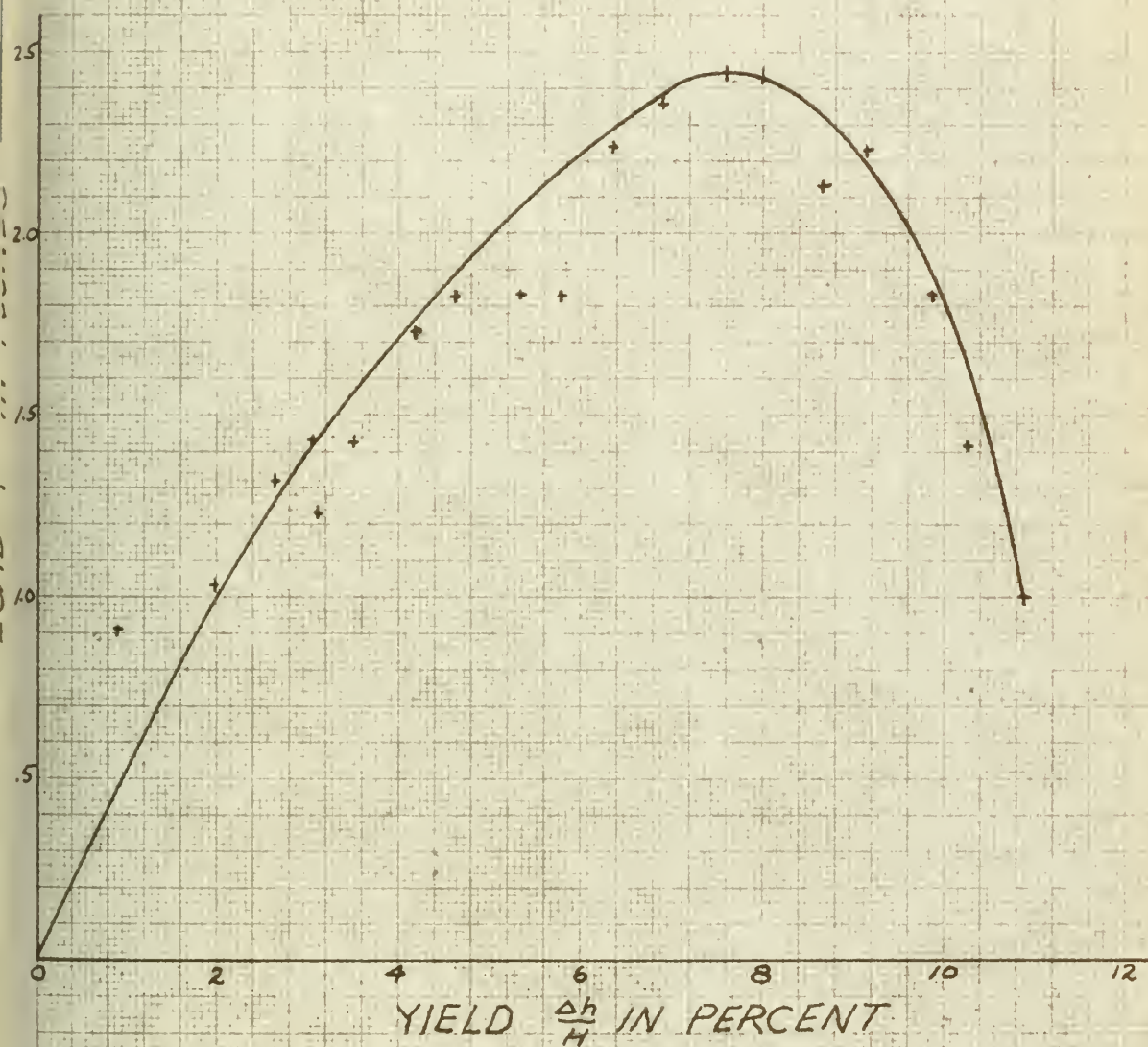
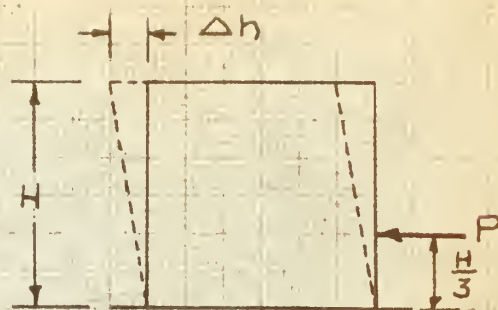


FIGURE XXIII LOAD AND YIELD CURVE (TEST #2)

TEST 3

The purpose of this test was to duplicate the effects attained in tests 1 and 2 respectively. Therefore, this test was conducted under the same identical conditions as described in the preceeding section except that the base of the model was restrained by a C - clamp and remained in a horizontal position throughout the test.

Photographic sequences resulting from this test are shown in Figure XXIV. Corresponding tabulated raw data are contained in the appendix.

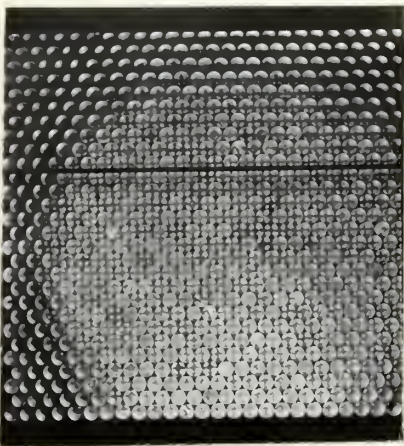


Figure XXIV a

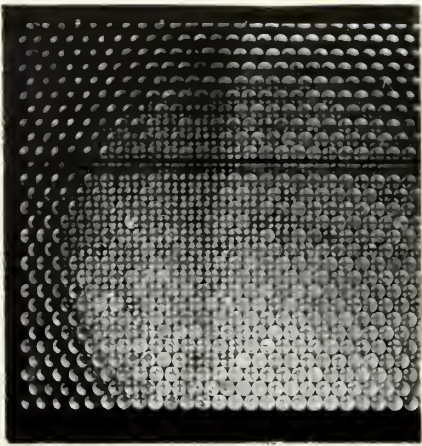


Figure XXIV b

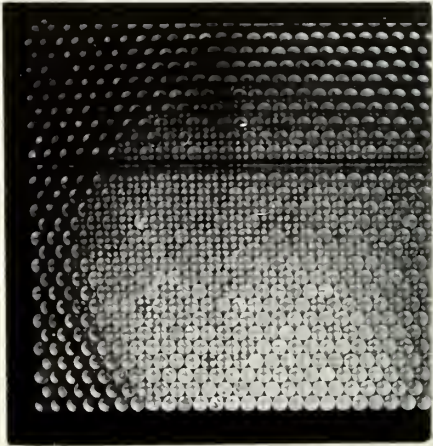


Figure XXIV c

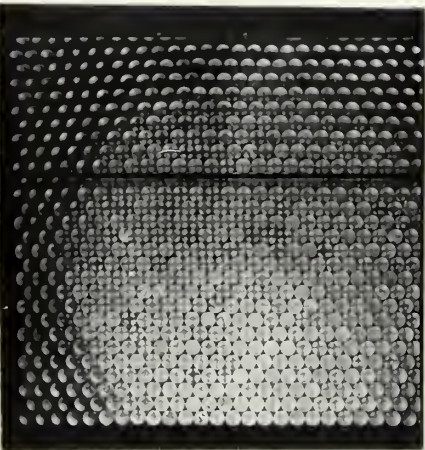


Figure XXIV d

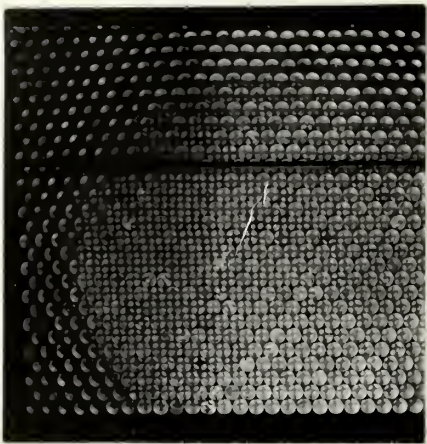


Figure XXIV e

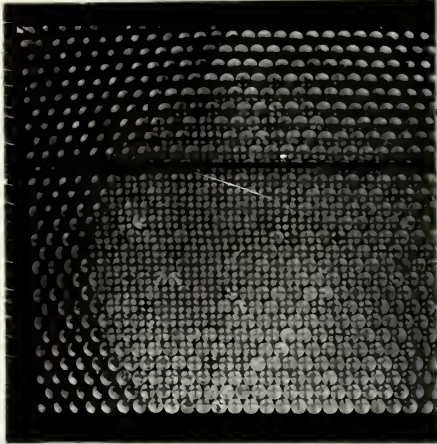


Figure XXIV f

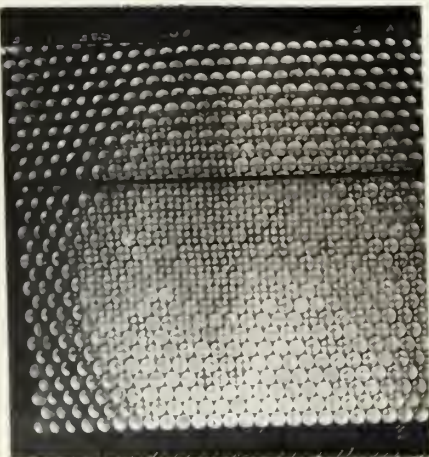


Figure XXIV g

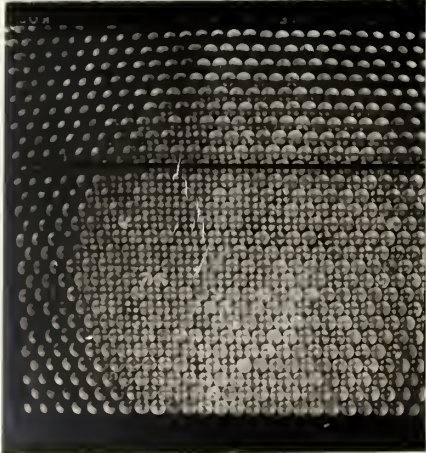


Figure XXIV h

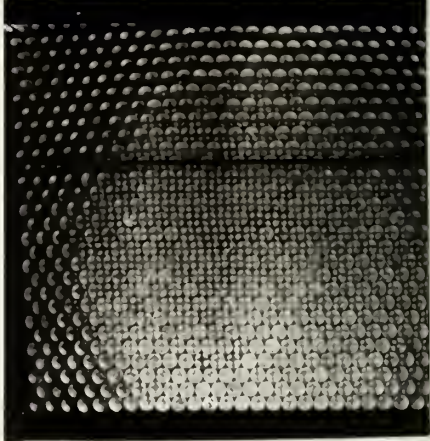


Figure XXIV i

Figure XXIV PHOTOGRAPHIC RESULTS - TEST 3

- Figure XXIV a No load condition with residual stresses in the cylinders.
- Load = 0.0 Lbs. Yield = 0.0 %
- Figure XXIV b Slight arching in center portion above horizontal reference line.
- Load = 1.0 Lbs. Yield = 0.8 %
- Figure XXIV c Arching progresses in central portion. Cylinders adjacent to unloaded wall remain intact.
- Load = 1.7 Lbs. Yield = 1.8 %
- Figure XXIV d Arching progresses in vertical direction.
- Load = 2.2 Lbs. Yield = 2.9 %
- Figure XXIV e Cylinders in right lower section begin to displace in a horizontal direction to the left.
- Load = 2.1 Lbs. Yield = 3.9 %
- Figure XXIV f Arching developed to lower quarter portion of photographs.
- Load = 2.1 Lbs. Yield = 4.7 %
- Figure XXIV g Pronounced displacement of cylinders in right portion of photograph.
- Load = 2.1 Lbs. Yield = 5.2 %
- Figure XXIV h Pronounced "wave" action with a crest in the central portion.
- Load = 2.1 Lbs. Yield = 5.5 %
- Figure XXIV i Progressive wave action continues.
- Load = 2.3 Lbs. Yield = 5.9 %

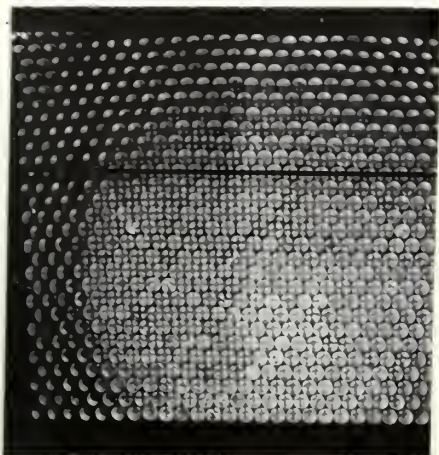


Figure XXIV j

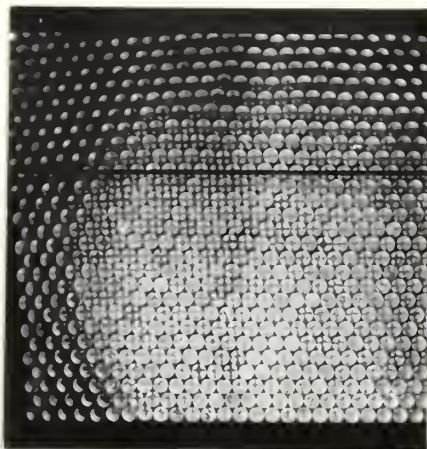


Figure XXIV k

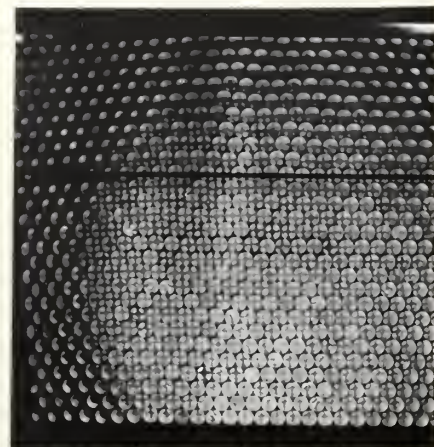


Figure XXIV l

Figure XXIV PHOTOGRAPHIC RESULTS - TEST 3 (CONTINUED)

Figure XXIV j Failure planes appear making an angle of approximately 62° with the horizontal. Second wave crest appears in center portion.

Load = 2.3 Lbs.

Yield = 6.6 %

Figure XXIV k Pronounced failure planes extend through the wave crests.

Load = 2.1 Lbs.

Yield = 7.4 %

Figure XXIV l Failure planes with extensive separations of cylinders in central portion.

Load = 1.9 Lbs.

Yield = 7.8 %

DISCUSSION

In general, the effects produced in this test were similar to those produced in the previous tests. The load versus yield curve, shown in Figure XXV, indicates that the peak of the curve however, was slightly shifted to the left. The maximum ordinate was 2.1 pounds and the corresponding yield was in the neighborhood of 7 percent. The scattered points near the peak are primarily

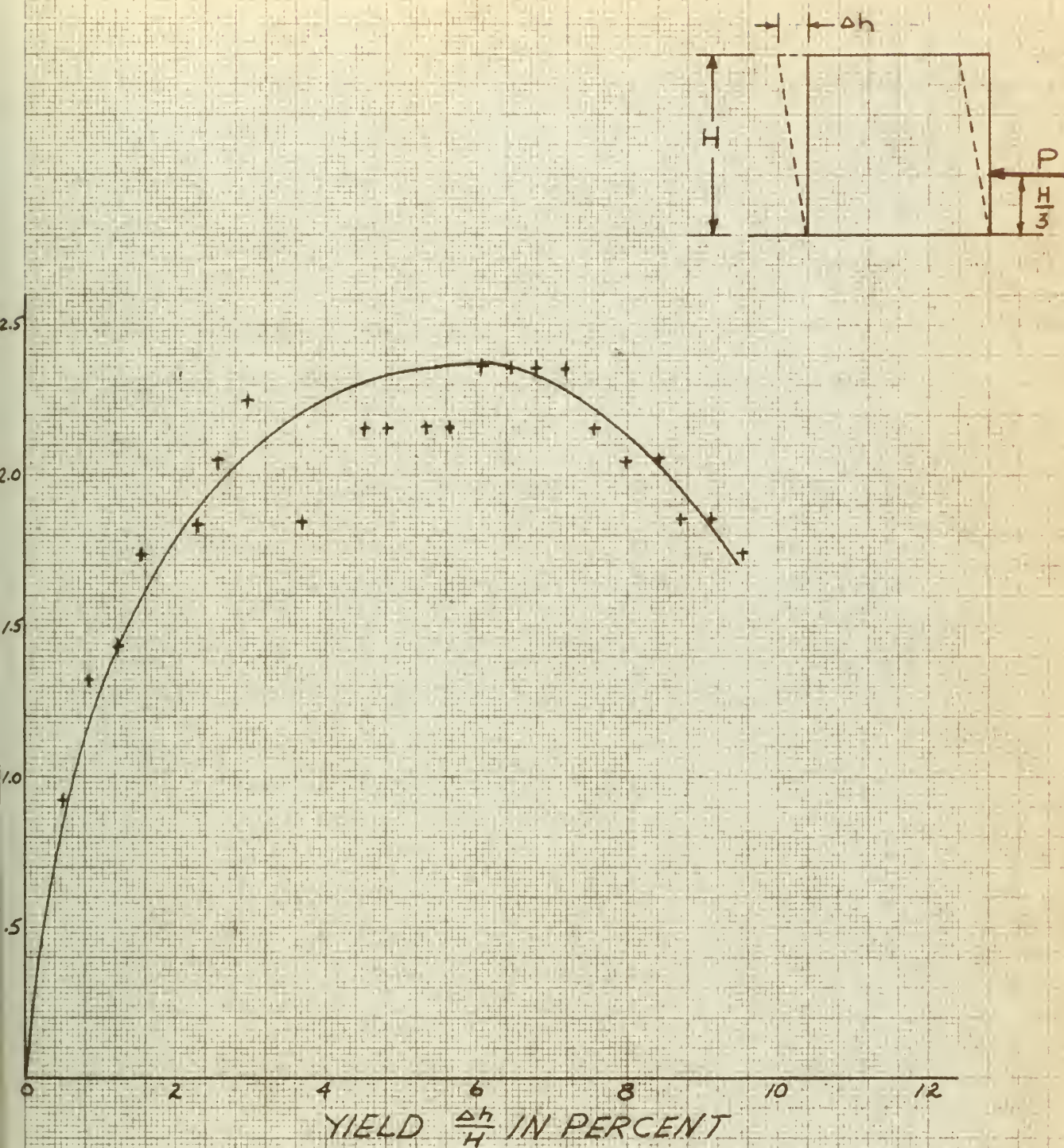


FIGURE XXV LOAD AND YIELD CURVE (TEST #3)

due to relaxation because the readings and photographs were taken at one minute intervals in this range.

A comparison of the three tests in the dense state indicates that the pronounced failure plane always occurred in the same vicinity. It started at the 1/4 point of the base of the model and extended to the surface at an angle of approximately 65° with the horizontal. The angle of this failure plane is principally due to the geometrical arrangement of the cylinders. However, it is believed that this would also be the angle of internal friction ϕ of the material. This could not be verified by a shear test because of the limited time available, it is worthy of further consideration.

A comparison of the curves indicates that there seems to be a linear relation between load and yield up to a yield value of about 2 percent. Beyond this the relationship is no longer linear.

TEST 4

The purpose of this test was to determine the distribution of stresses within the model when the cylinders are stacked in a loose condition - that is - each cylinder has four contact points as compared to six contact points in the dense state.

Testing procedure was identical to the one utilized in the dense state. The cylinders were stacked to a height of 2 inches below the crest of the model. This arrangement required 1444 cylinders. Essentially the porosity was increased by approximately 12 percent.

Preliminary tests revealed that most of the internal activity within the model occurred in a region extending from the loading wall toward the center of the model. As a result the photographs were taken to include the loaded wall as the right boundary, the base of the model as the lower boundary and include approximately 70 Percent of the model. Photographic results are shown in Figure XXVI. Tabulated raw data are found in the Appendix.

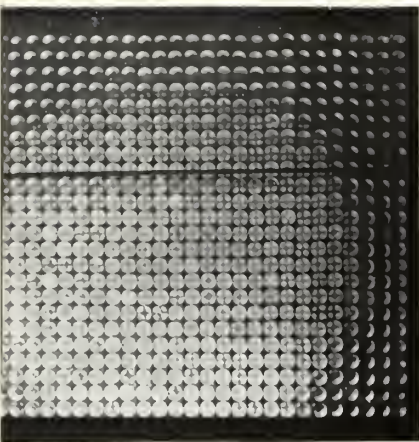


Figure XXVI a

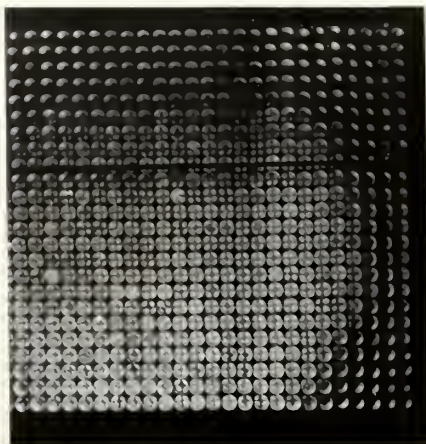


Figure XXVI b

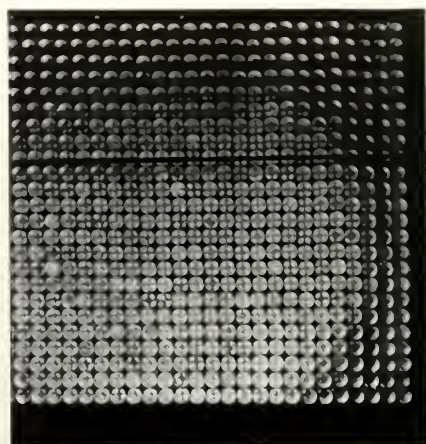


Figure XXVI c

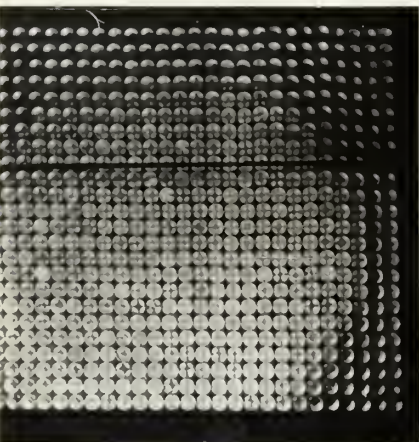


Figure XXVI d

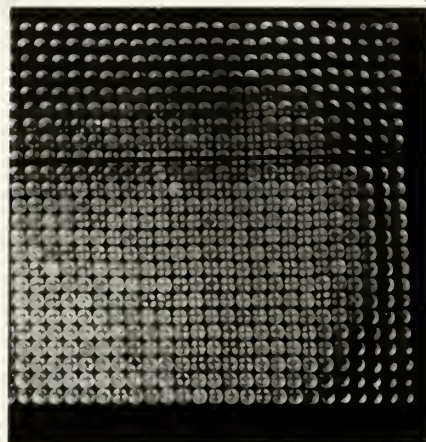


Figure XXVI e

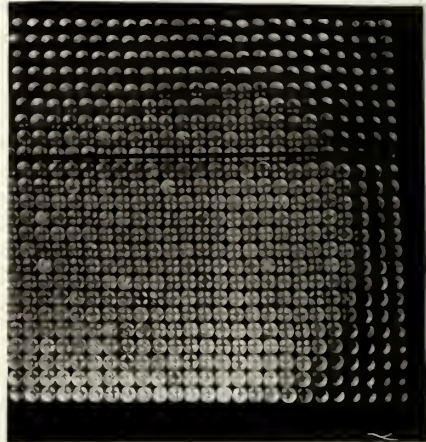


Figure XXVI f

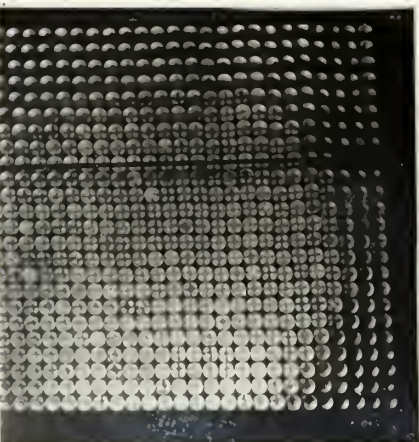


Figure XXVI g

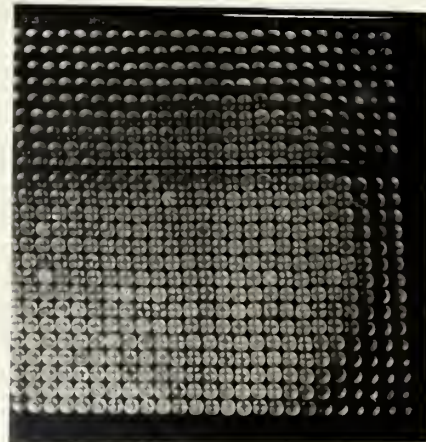


Figure XXVI h

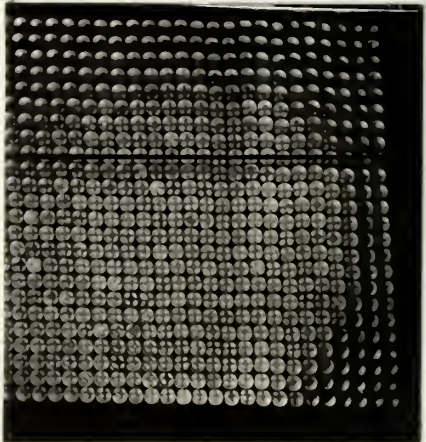


Figure XXVI i

Figure XXVI PHOTOGRAPHIC RESULTS - TEST 4

- Figure XXVI a No load condition with residual stress patterns.
 Load = 0.0 Lbs. Yield = 0.0 %
- Figure XXVI b Load = 0.3 Lbs. Yield = 0.6 %
- Figure XXVI c Load = 0.3 Lbs. Yield = 1.3 %
- Figure XXVI d Noticeable leaning of all cylinders to the left.
 Load = 0.2 Lbs. Yield = 2.4 %
- Figure XXVI e Slight arching near loaded wall.
 Load = 0.1 Lbs. Yield = 3.2 %
- Figure XXVI f Load = 0.1 Lbs. Yield = 3.9 %
- Figure XXVI g Arching increasing in vertical direction above horizontal reference line.
 Load = 0.1 Lbs. Yield = 4.7 %
- Figure XXVI h Cylinders in vicinity of horizontal reference line begin "rolling" movement to the left.
 Load = 0.0 Lbs. Yield = 5.5 %
- Figure XXVI i Arching progresses below horizontal reference line.
 Load = 0.1 Lbs.(compression) Yield = 6.7 %



Figure XXVI j



Figure XXVI k



Figure XXVI l

Figure XXVI PHOTOGRAPHIC RESULTS - TEST 4 (CONTINUED)

Figure XXVI j Sudden failure of model accompanied by extensive inward movement of loaded wall. Inclined failure plane at approximately 62° with horizontal base. Visible horizontal failure planes in vicinity of base.

Load = unknown Yield = 8.4 %

Figure XXVI k Top surface immediately adjacent to loaded wall.

Figure XXVI l Middle third section of model adjacent to loaded wall.

DISCUSSION

During the initial stages of loading, continuous observation of the cylinders revealed that the cylinders would "lean" toward the left as the amount of yield increased. At a load of .1 pounds and a corresponding yield of 3.2 percent slight arching appeared in the vicinity of the loaded wall. Progressive arching was subsequently accompanied by a "rolling" movement of the cylinders in the vicinity of the horizontal reference line. This effect increased in magnitude until a yield of approximately 8 percent was reached. At this point sudden failure occurred as shown in Figure XXVI j.

The extensive wall displacement which occurred between Figures XXVI i and XXVI j respectively is due to the weight of the loaded wall. As shown in the tabulated values, the horizontal loading ring at this point was indicating a compressive force rather than a tensile force.

This failure was characterized by a downward displacement of the central portion of the model with a corresponding rise of the cylinders in a zone adjacent to the loaded wall. Extensive separation of the cylinders occurred in the lower third portion. The failure plane appears to follow a direction which is parallel to the loaded wall.

The relationship between the load and corresponding yield is shown in Figure XXVII. Values for the compressive force were interpolated from a calibration curve. Maximum ordinate for the tensile load was .3 pounds.

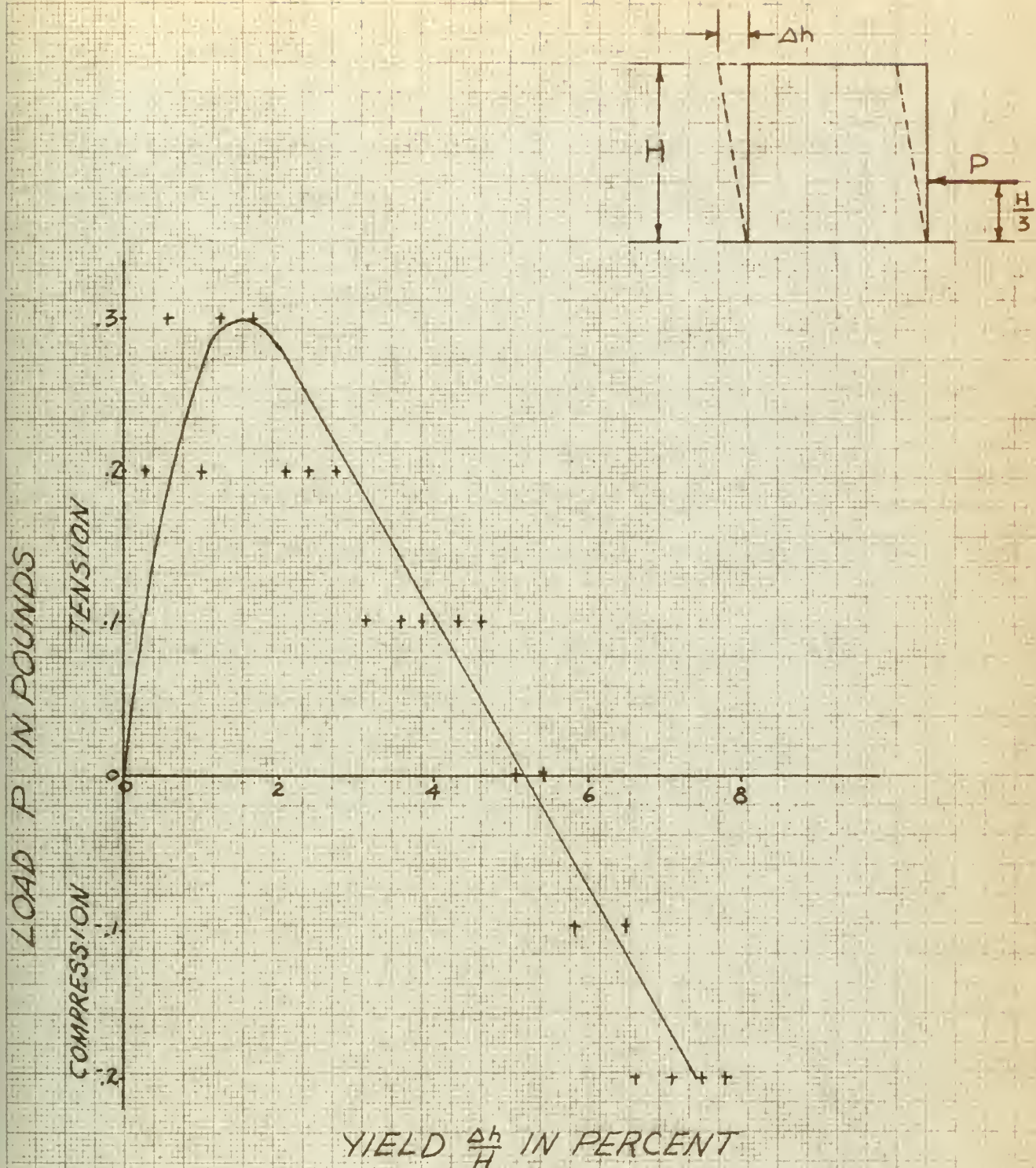


FIGURE XXVIII LOAD AND YIELD CURVE (TEST #4)

TEST 5

Since the weight of the loaded wall greatly influenced the mode of failure in test 4, the writer decided to conduct a test which would eliminate this effect. This was accomplished in the following manner:

1. A piece of strong, flexible twine was tied to the loaded wall near the top.
2. The twine ~~was~~ extended in a horizontal direction, normal to wall, to a distance of 18 inches. At this point it was supported by a 1/2 inch diameter rod, placed normal to the direction of the twine.
3. A 1 pound weight was attached at the other end of the twine.

Except for this slight modification, the testing procedure ~~was~~ the same as described in test 4.

Photographic results are shown in Figure XXVIII. The tabulated raw data sheets are found in the Appendix.

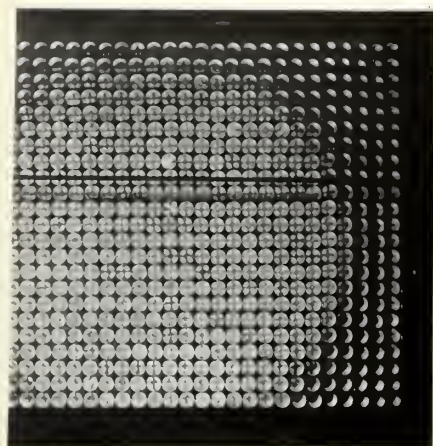


Figure XXVIII a

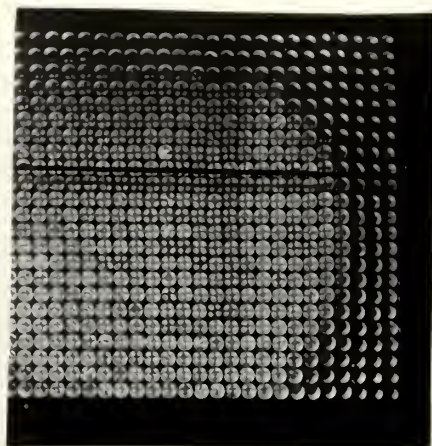


Figure XXVIII b

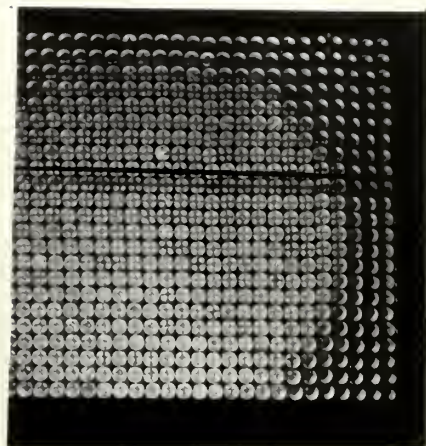


Figure XXVIII c

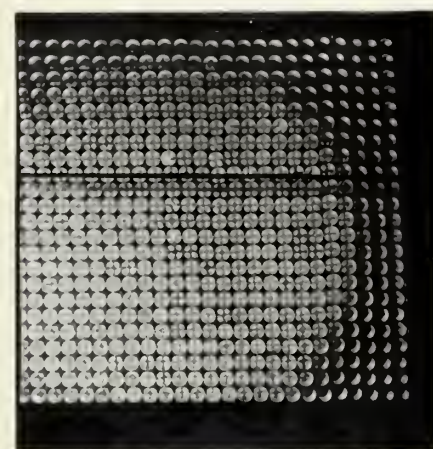


Figure XXVIII d

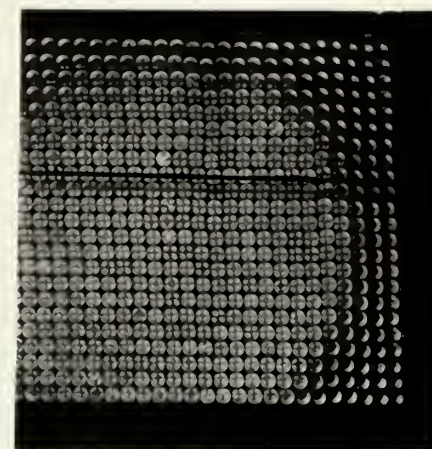


Figure XXVIII e

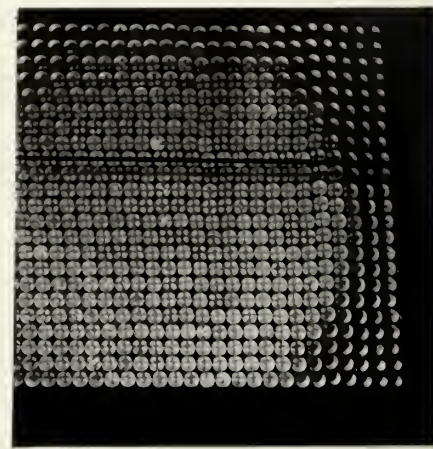


Figure XXVIII f

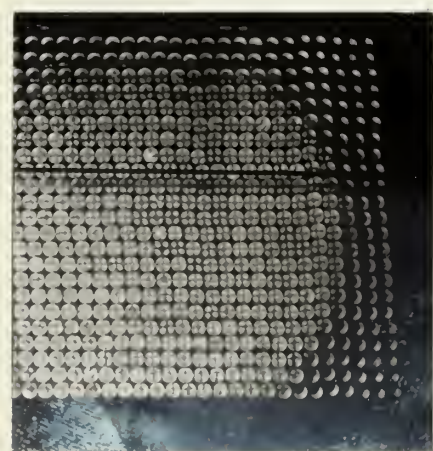


Figure XXVIII g

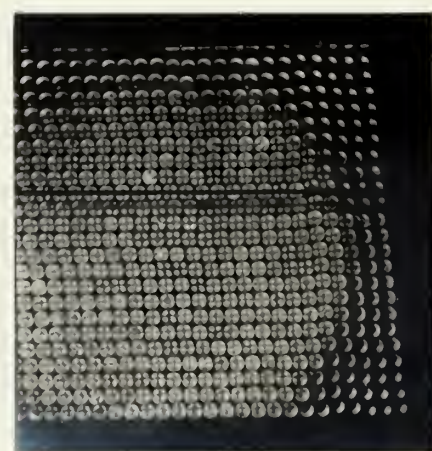


Figure XXVIII h

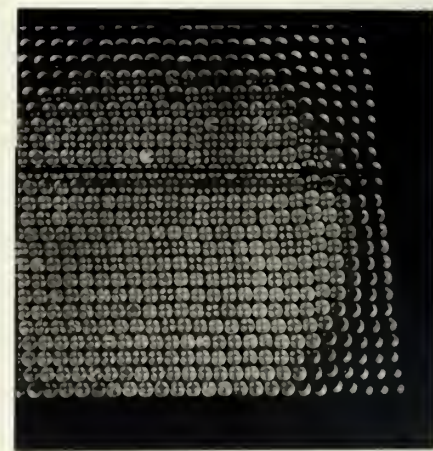


Figure XXVIII i

Figure XXVIII PHOTOGRAPHIC RESULTS - TEST 5

Figure XXVIII a No load condition with residual stress patterns.

Load = 0.0 Lbs. Yield = 0.0 %

Figure XXVIII b Load = 1.7 Lbs. Yield = 0.9 %

Figure XXVIII c Load = 2.9 Lbs. Yield = 2.1 %

Figure XXVIII d Noticeable shifting of cylinders to the left.

"Wave" begins to form near loaded wall.

Load = 3.7 Lbs. Yield = 3.3 %

Figure XXVIII e "Wave" action progresses to the left.

Load = 3.4 Lbs Yield = 4.5 %

Figure XXVIII f Load = 2.4 Lbs. Yield = 5.7 %

Figure XXVIII g Load = 2.1 Lbs Yield = 6.9 %

Figure XXVIII h Crest of "wave" increases near the loaded wall.

Load = 2.0 Lbs. Yield = 8.1 %

Figure XXVIII i Load = 2.3 Lbs. Yield = 9.3 %

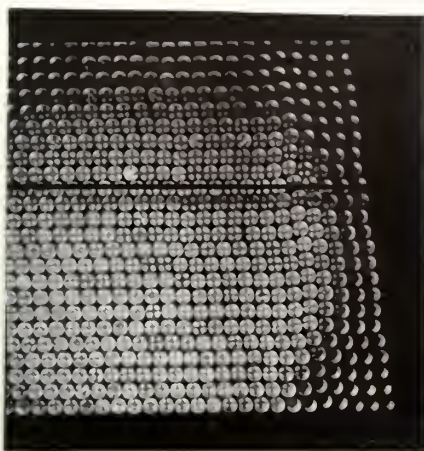


Figure XXVIII j

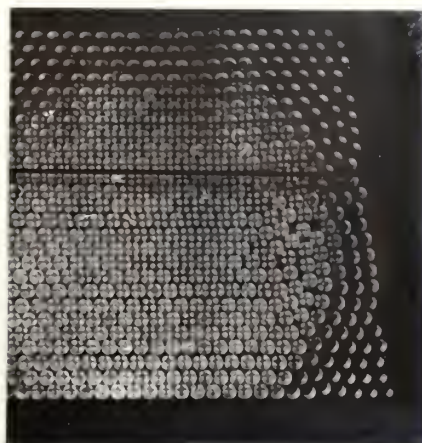


Figure XXVIII k

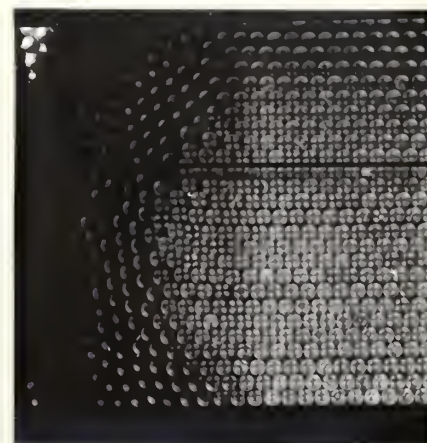


Figure XXVIII l

Figure XXVIII PHOTOGRAPHIC RESULTS - TEST 5 (CONTINUED)

Figure XXVIII j Noticeable separation of cylinders in central portion above horizontal reference line.

Load = 2.0 Lbs. Yield = 10.5 %

Figure XXVIII k Failure of fill material. Maximum separation of cylinders in vicinity of "wave" crest. Cylinders assume a dense state.

Load = unknown Yield = 11.7 %

Figure XXVIII l Position of cylinders near unloaded wall. Pronounced separation of cylinders along horizontal planes in central portion.

DISCUSSION

In general, the internal effects were similar to those observed in test 4. Arching began at a load of 3.7 pounds and a corresponding yield of 3.3 percent. As the yield increased the zone of arching also increased until a sudden failure occurred at a yield of 11.7 percent. *

The relationship between the load and corresponding yield

are shown in Figure XXIX. The average curve indicates that the relationship is approximately linear as the load approaches its maximum value. Beyond this point the relationship is no longer linear. For yield values greater than 10 percent the load remained constant at a value of 2.1 pounds. Larger loads were required because of the suspended weight and friction between the twine and supporting rod. Compressive forces were completely eliminated.

Although failure occurred in the vicinity of the arch, it was more noticeably complex than the failure observed in test 4. This verified the fact that the weight of the wall greatly influenced the manner of failure in test 4.

At failure, cylinders located at the surface of the model near the unloaded wall were at the same elevation as originally placed. The cylinders in the central portion shifted downward a distance of .75 inches while the cylinders near the loaded wall moved down a total distance of 1 inch from their original positions.

A comparison of both tests, in the loose state, revealed that the cylinders initially "lean" in a direction toward the unloaded wall as the yield was increased. The arching effect was then induced, which in turn was followed by a sudden failure in the vicinity of the arching zone.

These tests indicate that the failure, in a loose condition, was caused by the magnitude of the yield rather than the magnitude of the load.

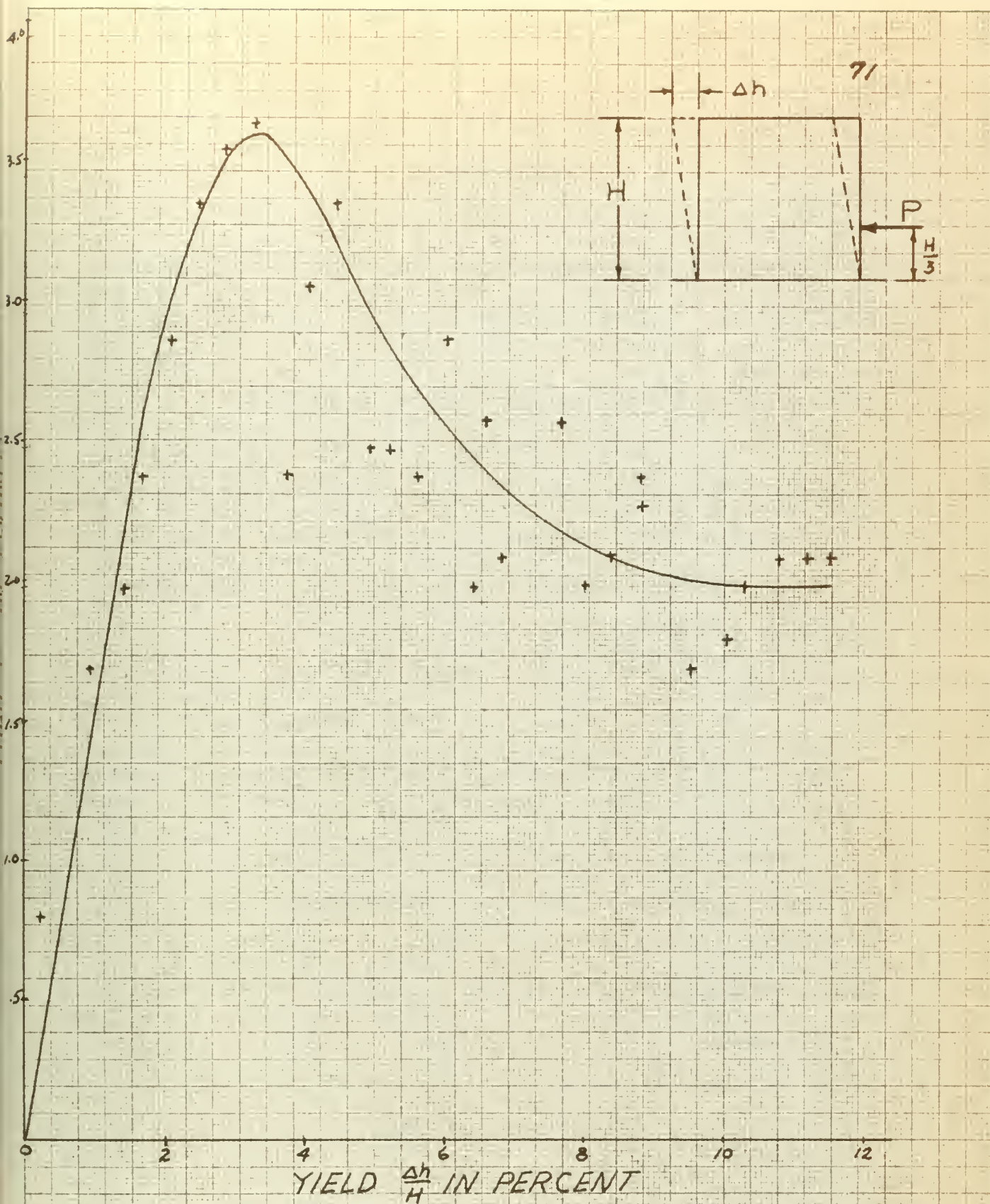


FIGURE XXIX LOAD AND YIELD CURVE (TEST "5")

PART VI

CONCLUSIONS

This section of the study is concerned with the conclusions reached after consideration had been given to the results of this study superimposed on the information available in the literature cited.

Attention is invited to the fact that this study was of a basic nature and that the time available for its accomplishment precluded the number of tests that could be conducted. Therefore, the conclusions listed below are based on a limited number of tests and are presented in general terms, as tentative.

1. Photoelastic analysis can be successfully applied in the study of shear stresses within the fill material in cofferdams.
2. In the dense state, two directions of failure were noticed, namely - one inclined at an angle of approximately 65° with the horizontal, and the other in a horizontal direction. The former began at the $1/4$ point of the base from the unloaded wall and extended to the surface. The latter extended from the loaded wall and terminated at the inclined failure plane.
3. The inclined failure planes passed through the crest of the "waves" which were formed.
4. Failure in the dense state is primarily controlled by the magnitude of the applied load, whereas the failure in a loose state is primarily due to the yield magnitude.

5. In the dense state three zones are formed. Zone one near the unloaded wall is wedge shaped and moves as a unit. Zone two, which is located in the central portion, contains the pronounced failure plane resulting from a collapsed arching effect. Finally, the third zone near the loaded wall contains horizontal failure planes.
6. Failure of the fill material placed in a loose condition is more complex than that of the fill material placed in a dense state.

PART VII
RECOMMENDATIONS

The author recommends continued study of this type aimed at a quantitative analysis based on the following suggestions:

1. Polishing the ends of the cylinders.
2. Refinement of the polariscope to include:
 - a. more intense light source with appropriate diffuser to increase the range of uniform, parallel, light rays.
 - b. use of monochromatic light.
3. Statistical arrangement of homogeneous cylinders.
4. Use of assorted diameter sizes to include the effect of particle size.
5. Conduct similar tests with a uniform surcharge.
6. Evaluate the angle of internal friction of the material.
7. Construct a model with both hinges on the outside of the vertical walls.
8. Use a motion picture camera to eliminate the effect of relaxation.
9. Utilizing a model with flexible walls.

PART VIII

LITERATURE CITED

1. ANDERSON, P., Substructure Analysis and Design, 2nd Edition,
The Ronald Press Company, New York, 1956.
2. BRAITZ, J.H.A., Stress Function of Photoelasticity Applied to
Dams, Proceedings of American Society of Civil Engineers,
Volume 61, p. 983, 1936
3. COLBURN, R.T., Sheet Pile Cofferdams and Test Cells for T.V.A.
Projects, Civil Engineering, September, 1939.
4. CUMMINGS, E.M., Cellular Cofferdams and Docks, Journal of the
Waterways and Harbor Division, Proceedings of the
American Society of Civil Engineers, Paper 1366,
September 1957.
5. CURTISS, A.J. and RICHART, F.E., Photoelastic Analogy for Non-
homogeneous Foundations, Proceedings of American Society
of Civil Engineers, Volume 79, Separate 211, July 1953.
6. DANTU, P., A Contribution to the Mechanical and Geometrical
Study of Non-cohesive Masses, Proceedings of the
4th International Conference on Soil Mechanics and
Foundation Engineering, Volume I, pp. 144 - 148, 1957.
7. DUNHAM, C.E., Foundations of Structures, McGraw - Hill Book Co.
Inc., New York.
8. EPSTEIN H., Design of a Cellular Cofferdam, Proceedings of 17th.
Annual meeting, Highway Research Board, National
Research Council, Volume 17, pp. 481 - 493, 1937.

9. FARQUHARSON and HENNES, R.G., Gelatin Models for Photoelastic Analysis of Stress in Earth Masses, Civil Engineering Volume 4, pp. 211 - 214, 1940.
10. FROCHT, M.M., Photoelasticity, Volume I, Wiley and Sons, New York, 1941
11. HETENYI, M., Handbook of Experimental Stress Analysis.
12. KRYNINE, D.P., Photoelasticity in Foundation Studies, Proceedings of 14th. Eastern Photoelasticity Conference, p. 426, December 1941.
13. PENNOYER, R.P., Gravity Bulkheads and Cellular Cofferdams, Civil Engineering, Volume 4, pp. 301- 305, 1934.
14. PENNOYER, R.P. and HOCKENSMITH, G., Design of Steel Sheet Piling Cofferdams, Civil Engineering, Volume 5, p. 19, 1935.
15. Photoelasticity Research, Special Committee Proceedings of the American Society of Civil Engineers, Volume 59, No. 5, p. 814, 1933.
16. POLIVKA, J.J., Use of Photoelasticity in Analysis of Hyperstatic Structures, Proceedings of 13th. Eastern Photoelasticity Conference, pp. 57 - 61, June 1941.
17. SMITS, H.G., Photoelastic Determination of Shrinkage Stresses, Proceedings of the American Society of Civil Engineers, Volume 61, p. 594, 1936.
18. TAN, EK KHOO, Stability of Soil Slopes, Transactions of American Society of Civil Engineers pp. 139 - 180, 1948.

19. TERZAGHI, K., Stability and Stiffness of Cellular Cofferdams,
Transactions of American Society of Civil Engineers,
Volume 110, p. 1083 with discussions, 1945.
20. TERZAGHI, K., Theoretical Soil Mechanics, Third printing,
John Wiley and Sons Inc., New York, 1946.
21. VERDEYEN, J., The Use of Flat Sheet Piling in Cellular
Construction, Proceedings of Second International
Conference on Soil Mechanics, Volume VII, p. 143, 1948.
22. WHITE and PRENTIS, Cofferdams, 2nd. edition, Columbia University,
Press, New York, 1950.

PART IX
APPENDIX

TABLE I

Time min.	Hor. Loading Ring in. $\times 10^{-3}$	Hor. Load lbs.	Hor. Dial Reading in. $\times 10^3$	Hor. Def. @ $\frac{1}{4}$ Pt. in.	Def. at Crest Δh in.	Yield $\frac{\Delta h}{H} \times 100$ %	Photo
0	0	0.0	0	.000	.000	0.0	1
2	93	0.8	84	.016	.064	0.6	2
4	91	0.9	64	.036	.144	1.2	3
6	89	1.0	45	.055	.220	1.9	4
8	88	1.3	25	.075	.300	2.6	5
10	89	1.0	4	.096	.384	3.3	6
12	89	1.0	81	.119	.476	4.1	7
14	88	1.3	62	.138	.552	4.8	8
16	88	1.3	42	.158	.632	5.5	9
18	87	1.4	21	.179	.716	6.2	10
21	85	1.7	89	.211	.844	7.3	
24	85	1.7	62	.238	.952	8.3	11
25	85	1.7	49	.251	1.004	8.7	
28	86	1.5	24	.276	1.104	9.6	
29	86	1.5	8	.292	1.168	10.2	12
31	93	0.8	87	.313	1.252	10.9	
32	93	0.8	76	.324	1.296	11.2	

REMARKS:

1. Horizontal deformation was read at the quarter point above the base and multiplied by 4 to indicate horizontal

TABLE I (CONTINUED)

deflection of the crest.

2. The following abbreviations have been used in all tables.

Hor. - Horizontal

Def. - Deformation

Min. - Minutes

In. - Inches

3. Computation for yield.

$$\text{Yield in percent} = \frac{\Delta h}{11.5 \text{ in.}} \times 100$$

4. These remarks are applicable to all tests.

TEST NUMBER 2

TABLE 2

Time min.	Hor. Loading Ring in. $\times 10^{-3}$	Hor. Load Lbs.	Hor. Dial Reading in. $\times 10^3$	Hor. Def. Pt. in.	Def. at Crest Δh in.	Yield $\frac{\Delta h}{H} \times 100$ %	Photo
0	0	0.0	0	.000	.000	0.0	1
3	91	0.9	74	.026	.104	0.9	2
6	89	1.0	43	.057	.228	1.9	3
7	88	1.3	32	.068	.272	2.6	
9	87	1.4	13	.087	.348	3.0	4
10	87	1.4	2	.098	.392	3.4	
12	86	1.7	82	.118	.472	4.1	5
13	84	1.8	71	.129	.516	4.5	
15	84	1.8	50	.150	.600	5.2	6
16	84	1.8	40	.160	.640	5.6	
18	82	2.2	20	.180	.720	6.2	7
19	80	2.3	8	.192	.768	6.7	
21	79	2.4	87	.213	.852	7.4	8
22	79	2.4	76	.224	.896	7.8	
24	81	2.1	56	.244	.976	8.4	9
25	82	2.2	45	.255	1.020	8.9	10
27	84	1.8	24	.276	1.104	9.6	11
28	87	1.4	13	.287	1.148	10.0	
30	89	1.0	94	.306	1.224	10.6	12

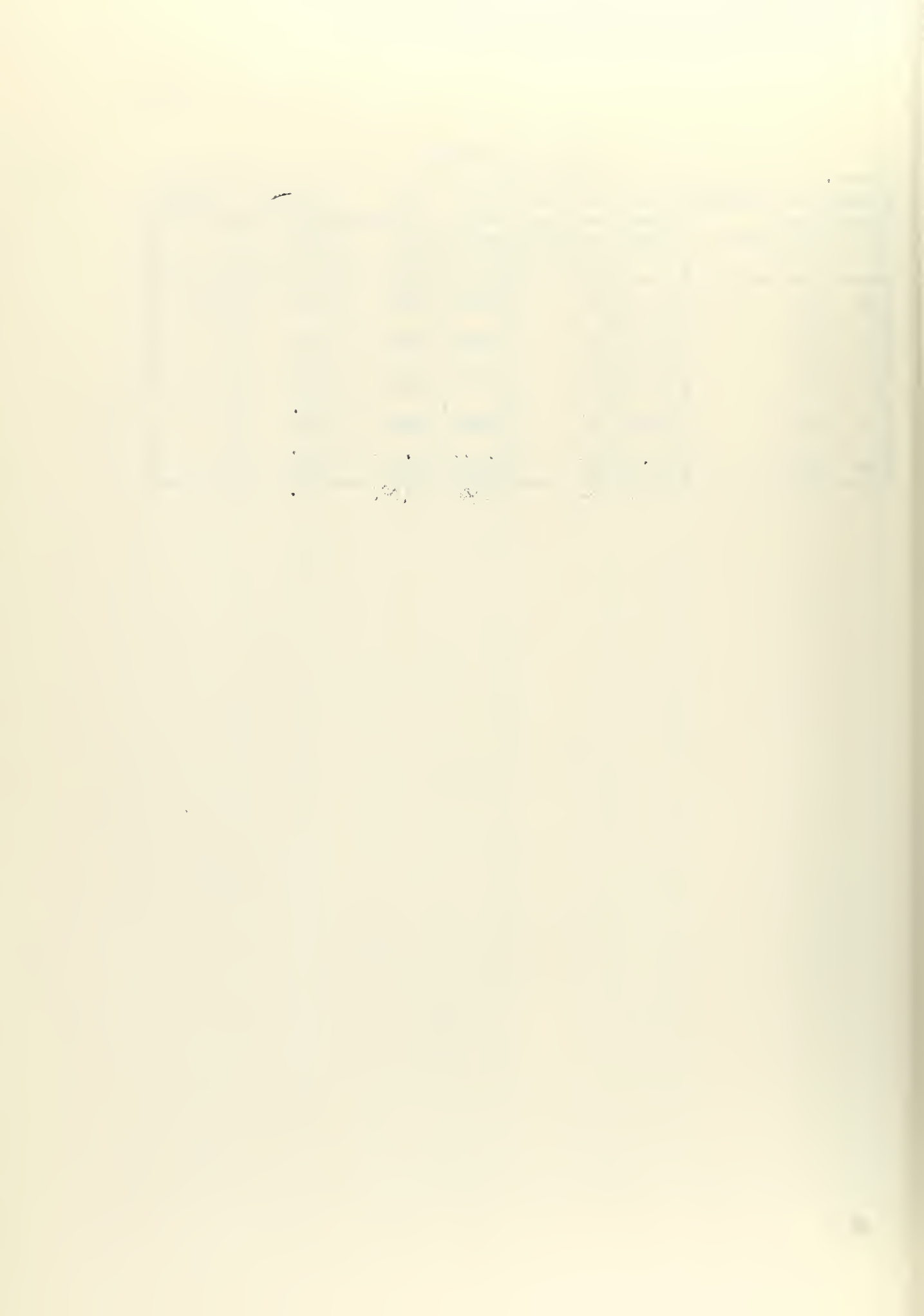
TEST NUMBER 3

TABLE 3

Time min.	Hor. Loading Ring in. x 10^3	Hor. Load Lbs.	Hor. Dial Reading in. x 10^3	Hor. Def. Pt. in.	Def. at Crest Δh in.	Yield $\frac{\Delta h}{H} \times 100$ %	Photo
0	0	0.0	0	.000	.000	0.0	1
2	91	0.9	86	.014	.056	0.5	
3	88	1.3	77	.023	.092	0.8	2
4	87	1.4	67	.033	.132	1.2	
5	85	1.7	57	.043	.172	1.5	
6	85	1.7	47	.053	.212	1.8	3
7	84	1.8	37	.063	.252	2.2	
8	83	2.0	27	.073	.292	2.5	
9	82	2.2	17	.083	.332	2.9	4
10	82	2.2	7	.093	.372	3.2	
11	84	1.8	95	.105	.420	3.6	
12	81	2.1	86	.114	.451	3.9	5
13	81	2.1	75	.125	.500	4.4	
14	81	2.1	64	.136	.544	4.7	6
15	81	2.1	52	.148	.592	5.2	7
16	81	2.1	41	.159	.636	5.5	8
17	80	1.3	30	.170	.680	5.9	9
18	80	2.3	19	.181	.720	6.3	
19	80	2.3	9	.191	.764	6.6	10
20	80	2.3	98	.202	.808	7.0	
21	81	2.1	88	.212	.848	7.4	11

TABLE 3 (CONTINUED)

Time min.	Hor. Loading Ring in. x 10^3	Hor. Load Lbs.	Hor. Dial Reading in. x 10^3	Hor. Def. @ 1 Pt. in.	Def. at Crest Δh in.	Yield $\frac{\Delta h}{H} \times 100$ %	Photo
22	83	2.0	76	.224	.896	7.8	12
23	83	2.0	66	.234	.936	8.2	
24	84	1.8	57	.243	.972	8.5	
25	84	1.8	45	.255	1.020	8.9	
26	86	1.7	35	.265	1.060	9.3	



TEST NUMBER 4

TABLE 4

Time min.	Hor. Loading Ring in. x 10^{-3}	Hor. Load Lbs.	Hor. Dial Reading in. x 10^{-3}	Hor. Def. opt. in.	Def. at Crest Δh in.	Yield $\frac{\Delta h}{H} \times 100$ %	Photo
0	0	.0	0	.000	.000	0.0	1
1	98	.2	92	.008	.032	0.3	
2	97	.3	82	.018	.072	0.6	2
3	98	.2	71	.029	.116	1.0	
4	97	.3	62	.038	.152	1.3	3
5	97	.3	51	.049	.196	1.7	
6	98	.2	40	.060	.240	2.1	
7	98	.2	31	.069	.276	2.4	4
8	98	.2	18	.082	.328	2.8	
9	99	.1	7	.093	.372	3.2	5
10	99	.1	95	.105	.420	3.6	
11	99	.1	86	.114	.456	3.9	6
12	99	.1	73	.127	.508	4.4	
13	99	.1	64	.136	.544	4.7	7
14	0	0	52	.148	.592	5.1	
15	0	0	41	.159	.636	5.5	8
16	-1	-.1	29	.171	.684	5.9	
17	-1	-.1	17	.189	.756	6.6	
18	-2	-.2	7	.193	.772	6.7	9
19	-2	-.2	91	.209	.836	7.2	
20	-2	-.2	81	.219	.876	7.6	

TABLE 4 (CONTINUED)

Time min.	Hor. Loading Ring in. x 10^3	Hor. Load Lbs.	Hor. Dial Reading in. x 10^3	Hor. Def. @ pt. in.	Def. at Crest Δh in.	Yield $\frac{\Delta h}{H} \times 100$ %	Photo
21	-2	-.2	71	.229	.916	7.9	
22	-	-	60	.240	.960	8.4	10

REMARKS:

1. Negative forces are compressive forces.

TEST NUMBER 5

TABLE 5

Time min.	Hor. Loading Ring in. x 10^3	Hor. Load lbs.	Hor. Dial Reading in. x 10^3	Hor. Def. @ 1 Pt. in.	Def. at Crest Δh in.	Yield $\frac{\Delta h}{H} \times 100$ %	Photo
0	0	0.0	0	.000	.000	0.0	1
1	92	0.8	93	.007	.028	0.2	
2	89	1.0	82	.018	.072	0.6	
3	85	1.7	72	.028	.112	0.9	2
4	83	2.0	61	.039	.156	1.4	
5	79	2.4	50	.050	.200	1.7	
6	76	2.9	40	.060	.240	2.1	3
7	72	3.4	28	.072	.288	2.5	
8	70	3.6	17	.083	.332	2.9	
9	69	3.7	4	.096	.384	3.3	4
10	79	2.4	91	.109	.436	3.8	
11	74	3.1	81	.119	.476	4.1	
12	72	3.4	70	.130	.520	4.5	5
13	78	2.5	57	.143	.572	5.0	
14	78	2.5	47	.153	.612	5.3	
15	79	2.4	36	.164	.656	5.7	6
16	76	2.9	23	.177	.708	6.1	
17	83	2.0	12	.188	.752	6.5	
18	81	2.1	1	.199	.796	6.9	7
19	77	2.6	89	.211	.844	7.3	
20	77	2.6	77	.223	.892	7.8	

TABLE 5 (CONTINUED)

Time min.	Hor. Loading Ring in. x 10^3	Hor. Load Lbs.	Hor. Dial Reading in. x 10^3	Hor. Def. @ Pt. in.	Def. at Crest Δh in.	Yield $\frac{\Delta h}{H} \times 100$ %	Photo
21	83	2.0	66	.234	.936	8.1	8
22	81	2.1	54	.246	.984	8.5	
23	79	2.4	42	.258	1.032	8.9	
24	80	2.3	32	.268	1.072	9.3	9
25	85	1.7	19	.281	1.124	9.7	
26	84	1.8	8	.292	1.168	10.2	
27	83	2.0	96	.304	1.216	10.5	10
28	81	2.1	85	.315	1.260	11.0	
29	81	2.1	73	.327	1.308	11.4	
30	81	2.1	61	.339	1.356	11.7	11

CALIBRATION CURVE
FOR PROVING RING
(TENSILE FORCE VS. DIAL READING)

FIGURE XXX



TECHNICAL DATA

Hysol 6000A is a synthetic material based on epoxy resins which are thermosetting in nature. The permeability of moisture vapor is low and freedom from internal strains is exceptional. They possess excellent dimensional stability.

1. Color - 6000A - Transparent amber
2. Specific gravity - 1.21
3. Tensile strength psi. - 12,200
4. Compressive strength psi. - 12,200
5. Modulus of Elasticity psi. - $.455 \times 10^6$
6. Water absorption % 6 months - .09

MACHINING HYSOL CAST EPOXY RESINS

Hysol materials can be machined with excellent results using standard machine shop equipment.

GENERAL SUGGESTIONS

1. Medium to high speeds with low rates of feed.
2. Carbide tipped tools
3. Correct grinding of cutting tools
4. Stone tool to remove feather edge, or work will chatter and chip.
5. Support work to prevent material from flexing or springing away.
6. Control heat buildup.

Sawing For general purposes, 12 to 14 teeth per inch is satisfactory. Thickness of piece will govern the selection of the

saw and number of teeth. Cutting may be done with a cut-off wheel such as Carborundums' A24-R-Fx2RS, 3/32" thick by 10" diameter or Carborundums' TC60-Q-B5.

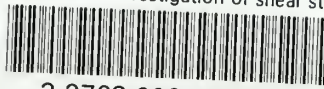
Milling, shaping, et cetera may also be performed. The operator or machinist can best determine the type and style of tool, depending on equipment available and results required.





thesG51

Photoelastic investigation of shear stre



3 2768 002 02954 8

DUDLEY KNOX LIBRARY